



## Invited Review

## A review of laser-induced breakdown spectroscopy and spontaneous emission techniques in monitoring thermal conversion of fuels

Meirong Dong<sup>a,b,\*</sup>, Junbin Cai<sup>a,b</sup>, Hongchuan Liu<sup>a,b</sup>, Junchang Xiong<sup>a,b</sup>, Gangfu Rao<sup>a,b</sup>, Shunchun Yao<sup>a,b</sup>, Jidong Lu<sup>a,b</sup><sup>a</sup> School of Electric Power, South China University of Technology, Guangzhou, Guangdong 510640, China<sup>b</sup> Guangdong Province Engineering Research Center of High Efficient and Low Pollution Energy Conversion, Guangzhou, Guangdong 510640, China

## ARTICLE INFO

## Keywords:

Thermal conversion  
Laser-induced breakdown spectroscopy  
Spontaneous emission  
Energy materials  
Combustion flame  
Fly ash

## ABSTRACT

Thermal conversion, such as combustion, is the basic utilization of fuel energy. In-situ detection of key parameters (e.g., components of fuel and combustion products, temperature, and pressure) is critical for improving the fuel utilization and the efficiency of thermal conversion equipment as well as to gain a full understanding of the mechanism of the thermal conversion process. Laser-induced breakdown spectroscopy (LIBS) has been verified to be applicable in the relevant industrial environment. In addition, combustion inherently comes with spontaneous emission, which contains important information about the process. This review discusses the application of atomic emission spectroscopy for monitoring the fuel thermal conversion process, including the characterization of raw energy materials (coal, biomass) before combustion, during the fuel combustion process (flame) and after combustion (fly ash). The first section is focused on LIBS for the analysis of raw energy materials in different forms like rock, pellets and particle flow. A series of online application instruments for energy materials properties analysis have been developed. The second section is focused on the characterization of the fuel combustion process with the use of LIBS and spontaneous emission. The third section is on unburned carbon detection in fly ash with LIBS. Furthermore, application prospects of LIBS and spontaneous emission techniques in the energy conversion field are analyzed and discussed to provide a reference for the development of technology.

## 1. Introduction

## 1.1. Overview

Energy is an important guarantee for achieving sustainable economic development, and it is also the basis for human survival. According to the British Petroleum (BP) statistical review of world energy 2022, coal is an important energy material and accounted for 29.3% of the world's total primary energy consumption in 2021 [1]. Recently, the proportions of biomass and other new energy sources have increased, which promotes the diversification of energy structure. Clean utilization of fuels includes physical conversion, biochemical conversion, and thermochemical conversion to convert raw energy materials into electricity, heat, gas, liquid fuels or high valued chemicals. Thermochemical conversion is simple and easily controllable because of its fast reaction and high energy utilization rate. As such, it is the main mode of energy supply in the world. Thermochemical conversion methods mainly

include combustion, liquefaction, hydrothermal upgrading technology, gasification, and pyrolysis [2–5]. Although combustion inherently produces a variety of pollutants, it is still the basic method for fuel heat utilization, for example in power production, heating, and transportation.

The boiler is common, high-energy-consumption equipment for energy conversion. It provides a high-temperature and high-pressure water/steam for community and industry through fuel combustion, which involves the flow field, heat and mass transfer, and chemical reactions. With the development of large-scale, multiple-parameter, and digital energy conversion systems, like supercritical or ultra-supercritical thermal power generating units, stringent requirements are put forward for their safe and economic operations. Some key parameters are inter-dependent and related. Accordingly, system operation requires continuous real-time monitoring of material compositions before and after utilization (e.g., combustion products). In addition, for dynamic characterization of the combustion process, it is fundamental

\* Corresponding author.

E-mail address: [epdongmr@scut.edu.cn](mailto:epdongmr@scut.edu.cn) (M. Dong).<https://doi.org/10.1016/j.sab.2023.106807>

Received 4 February 2023; Received in revised form 9 October 2023; Accepted 11 October 2023

Available online 27 October 2023

0584-8547/© 2023 Elsevier B.V. All rights reserved.

to combine advanced measurement methods to better understand the combustion mechanism so as to master the underlying physical chemistry. Research in these aspects is of great significance for improving the utilization efficiency of fuel and reducing the generation of pollutants, especially under the growing concerns of climate change, low-carbon economy, sustainability, and environmental impact of conventional fuel usage.

### 1.2. The need for monitoring key parameters of an energy conversion system

Figure 1 shows a schematic diagram of a typical energy conversion system from fuel to electricity of a thermal power plant with coal combustion. The plant can be broken down into several main parts: coal conveyor, coal delivery system, boiler combustion system, steam and water system, flue gas pollutant treatment system, and power generation system. There are five main categories in status monitoring, and various sensors are responsible for their measurements: (1) temperature of steam and water system, flue gas system, heating surface tube wall; (2) pressure of steam and water system; (3) flow of feed water, steam, flue gas; (4) material composition of raw fuels, combustion products (fly ash, flue gas); and (5) others, for example, fuel particle size, control valve position. In this work, we focus on the material composition measurement of raw fuels and fly ash, and combustion diagnostics, and where indicated the suitable positions of different techniques (Fig. 1).

A modern distributed control system (DCS) is equipped to realize online data acquisition and remote automatic control of the equipment operation. However, some key parameters, for example, raw material characteristics and combustion products like unburned carbon in fly ash, still are obtained mostly through offline analysis and feedback to the DCS system through manual data entry. For the offline analysis method, the whole process of sampling, sample preparation and analysis usually takes several hours. The delayed results seriously lag behind the combustion conditions inside the boiler. The operation of coal-fired boilers could fail to properly adjust the combustion condition in time when the incoming coal or load fluctuates greatly, leading to increased incomplete combustion losses. Therefore, there is an urgent need to develop advanced and rapid (preferably real-time and online) analytical methods for material characterization before and after combustion.

Nowadays, the relatively mature, fast techniques for coal quality analysis mainly include X-ray fluorescence (XRF) [7,8] and prompt gamma neutron activation analysis (PGNAA) [9,10]. XRF can measure only elements with an atomic mass greater than 23, and its results are affected greatly by coal type. The PGNAA instrument is very bulky in size, involves the use of radioactive material, and has a high capital cost. These limitations hinder PGNAA from being more widely used for online field analysis of material quality. For composition analysis of fly ash, some common online analysis methods are based on the principles of microwave, optical reflection, infrared measurement, weight loss and radiation [11]. Although the microwave method is the most commonly used one for online measurement of unburned carbon, the analysis results are greatly affected by the fluctuations of power load and the types of coal [12,13].

Since the late 20th century, laser-induced breakdown spectroscopy (LIBS) has flourished rapidly and provides a potential new way for online characterization of material composition. Upon the action of a strong, focused pulsed laser beam, the specimen is partly evaporated, ionized and excited instantaneously. A transient, high-temperature plasma generates within the material vapor and the surrounding gas atmosphere. The identities of the elements and their concentrations can be inferred through measurement of the emission spectrum of the plasma [14–17]. Compared with other optical measurement techniques, LIBS is developing gradually into a highly competitive online detection technology for industrial processes by virtue of its advantages such as little sample pretreatment, minimal damage to samples, and simultaneous rapid detection of multiple elements. It has been developed for the quality control or status diagnostics of various industrial processes, for example, minerals [18,19], metallurgy [20,21] and nuclear engineering [22,23]. The superiority of LIBS over other measurement methods is especially highlighted in harsh industrial environments, for example, in combustion [24] and metallurgy [25]. This article reviews the diagnostic studies of LIBS in the energy conversion process, including raw energy materials (Section 2) and combustion products (Section 4).

### 1.3. The critical issue related to chemical analysis of the fuel thermal conversion process

Although combustion can provide energy for the development of

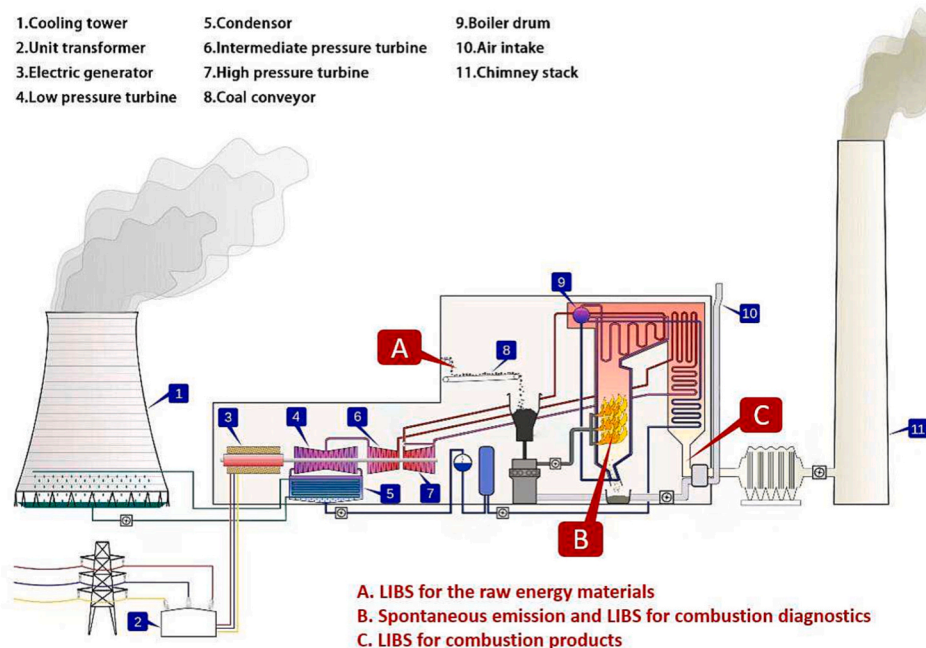


Fig. 1. Schematic diagram of a typical thermal power plant with LIBS and spontaneous emission techniques (modified) [6].

human society, it also brings with it a series of environmental issues. For example, solid fuel combustion generates CO, CO<sub>2</sub>, NO<sub>x</sub>, SO<sub>x</sub> and other harmful substances that affect human health and the environment. Alkali metals (Na and K) in fuels would be released during the combustion process and cause slagging on furnace walls and subsequently affect the heat transfer efficiency. Therefore, it is essential to fully characterize and understand the combustion mechanisms to achieve efficient and clean utilization of fuels.

There are several offline methods for studies on the thermal characteristics of solid fuels, such as the thermogravimetric analyzer (TGA/DTG), tube furnace (TF), wire mesh reactor (WMR), dropper furnace (DFT), high-temperature one-dimensional furnace (1D-EFR) and laminar flow flat flame burner (FFB). These techniques are available for a better understanding of the basic characteristics of the pyrolysis, gasification, and combustion process through the sampling analysis under a certain heating rate or temperature conditions. Recently, the use of sampling probes and the combination of other techniques, such as Fourier-transform infrared spectroscopy (FTIR) [26,27], mass spectrometry (MS) [28], and gas chromatography (GC) [29], results in the realization of real-time simultaneous analysis of products in the fuel thermal conversion process. Through correlations among temperature, flue gas compositions and the remaining ash components, a mechanism study can be performed to establish a reaction kinetic model, and the corresponding kinetic parameters are obtained. However, the detailed mechanistic cannot be obtained based on in-situ and intermediate product components along the thermal conversion process of fuels.

As a non-contact technique, optical measurement can provide in-situ continuous measurement of multiple parameters, which greatly improves the possibility of detecting active components or intermediates in complex processes and its adaptability in actual monitoring applications. With the development of computing technologies such as image processing and artificial intelligence, the optical measurement technology has been promoted and improved. At present, the common optical measurement methods used in the combustion field include emission spectroscopy and laser spectroscopy [30–32]. This review also focuses on the application of spontaneous emission and LIBS for combustion diagnostics (Section 3).

## 2. LIBS for raw energy materials

### 2.1. General

Coal and biomass are typical raw energy materials. Their properties generally include calorific value (or heat), proximate analysis (volatile matter, ash, moisture, and fixed carbon), ultimate analysis (C, H, O, N, and S), composition of ash (Al<sub>2</sub>O<sub>3</sub>, SiO<sub>2</sub>, Na<sub>2</sub>O, K<sub>2</sub>O, CaO, MgO, TiO<sub>2</sub>, and Fe<sub>2</sub>O<sub>3</sub>), and other characteristics related to heat utilization (e.g., slagging, ignition, burnout) [33–38]. For traditional offline analysis methods, most of the aforementioned properties are measured with different methods and with separate instruments. For example, the calorific value is obtained with a calorimeter, C and H contents are obtained with the combustion method, N content is analyzed via the semi-micro Kjeldahl method, S content is analyzed with an infrared sulfur analyzer, and proximate analysis indicators (volatile matter, ash, moisture) are obtained via industrial analyzers. Furthermore, there are multiple empirical correlations expressing the relation among the calorific value, proximate analysis, and ultimate analysis based on various basic assumptions.

LIBS, as a kind of atomic emission spectroscopy, obviously meets the analysis requirement of various elements, including metals and non-metals. Moreover, it has also been developed as a reliable technique for proximate analysis. To understand the laser interaction process and improve the accuracy of various indicators, relevant studies have been carried out, from fundamentals to industrial applications.

### 2.2. Fundamental issues of LIBS for detection of energy materials properties

C, H, O, N, and S are the main non-metallic elements and a significant part of macromolecular organic matter in energy materials. They are closely related to the combustion process. Fig. 2 presents the basic structural unit of coal with different coalification degrees (lignite, bituminous, and anthracite), which indicates that the molecular structure of coal at different coalification levels is distinct with diverse ways of atom connections [39]. During the process of laser ablation, the chemical bonds are broken and free atoms are formed and excited, which accompany radiative transition of the outer electrons (i.e., atomic emission). The different atomic arrangements in the sample would affect the excitation of elements and the interaction among the elements.

C, N, and O have high excitation potentials and low transition probabilities so that the intensity of their spectral lines is usually weak. Table 1 summarizes the characteristic wavelength and excitation energy level of these elements. Moreover, the atomic lines of most non-metallic elements are often located in the deep or even vacuum ultraviolet (UV) region or the near-infrared region (NIR), which increases measurement difficulty, especially for sulfur (S).

In addition, the forms of these non-metallic elements occurring in energy materials are complicated. Most of the hydrogen in coal exists in the form of organic matter, and some of it exists as moisture. Carbon is present mainly in organic form, with a small amount as inorganic carbonate. Sulfur content is mostly below 3%, but in three different forms: organic sulfur connected with hydrocarbon, inorganic sulfur as pyrite sulfide and sulfate, and a small amount as elemental sulfur. Their sum is called total sulfur. Likewise, oxygen has three occurrence forms: organic oxygen, mineral oxygen, and oxygen as moisture. The existence and correlation for all the non-metallic elements of coal are summarized in Fig. 3. Each element connected to carbon represents an organic form, and the dotted box represents the main composition of minerals. The ultimate analysis of solid fuel mainly refers to the content of these elements in organic form. Nevertheless, the plasma spectral information of related elements includes the sum of various morphological information, so that it is necessary to realize the identification of element morphology for high-precision quantitative analysis.

At present, there are only a few LIBS studies focusing on quantitative analysis of specific morphological elements in solid fuel. Zhang et al. [41] utilized LIBS technology to measure organic oxygen in anthracite coal in the atmospheric environment. In their approach, the atomic N line was selected as the internal standard line to establish a calibration curve for the total oxygen content. The content of inorganic oxygen was then acquired according to quantitative analysis of Si and Al by assuming that all the inorganic oxygen in coal is in the form of SiO<sub>2</sub> and Al<sub>2</sub>O<sub>3</sub>. Thereafter, the content of organic oxygen was inferred through the difference between the total oxygen and the inorganic oxygen. The measured relative standard deviation of organic oxygen was 19%. In another study, researchers attempted to identify carbon speciation based on molecular spectroscopy, and it was found that molecular spectra CN emission was strongly correlated with the carbon in organic form [42].

For the analysis of O and N, because they are the main constituents of air, the optical emissions would be significantly affected by interaction between the plasma plume and the ambient gas. Therefore, it is important to gauge the contribution of air to O and N emissions. Li et al. [43] found that the intensity of O I 777.4 nm from the coal sample was evidently higher in air than that in N<sub>2</sub>, indicating that the O emission originated from both coal and air. Wang et al. [44] compared the emission of three major elements, C, H, and N, in twenty-four bituminous coal samples under argon, helium, and air. The nitrogen emission was too weak to be detected in argon, indicating that the stronger N emission measured in the air condition was related to ambient N<sub>2</sub>.

Moreover, the evolution of plasma species is a complex dynamic process. Several studies clarified the formation route of species in

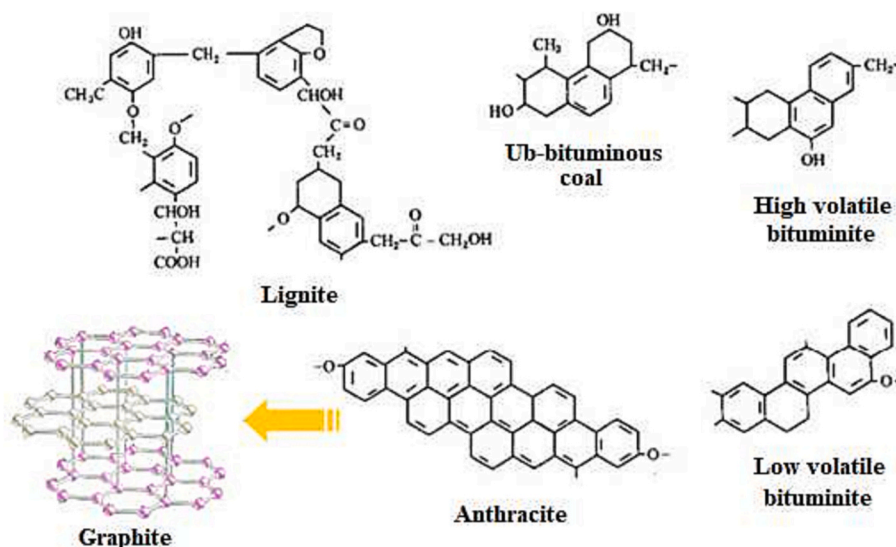


Fig. 2. Basic structural unit of coal with different coalification degrees.

Table 1  
Spectral and physical properties of nonmetal elements [40].

Spectral line	Wavelength (nm)	$E_i - E_k$ (eV)	Transition probability $A_{ki}$ ( $s^{-1}$ )
C I	193.091	1.264–7.685	$3.39 \times 10^8$
C I	247.856	2.684–7.685	$2.80 \times 10^7$
H $\beta$	486.130	10.199–12.749	$9.67 \times 10^6$
H $\alpha$	656.277	10.199–12.087	$2.24 \times 10^7$
N I	742.364	10.326–11.996	$5.64 \times 10^6$
N I	744.229	10.330–11.996	$1.19 \times 10^7$
N I	746.831	10.336–11.996	$1.96 \times 10^7$
O I	777.194	9.146–10.741	$3.69 \times 10^7$
O I	777.417	9.146–10.740	$3.69 \times 10^7$
O I	777.539	9.146–10.740	$3.69 \times 10^7$
Si I	191.470	0.049–6.524	$2.14 \times 10^4$
Si I	921.287	6.524–7.870	$2.79 \times 10^7$

is derived from  $C_2$  band emission, which is different from the excitation temperature due to the atoms' recombination processes. It is used to correct for plasma fluctuations. Based on this basic understanding, we proposed the method of combining atomic and molecular carbon emissions for the quantitative analysis of the carbon content in coal and achieved better measurement accuracy with  $R^2$ , RMSECV, and RMSEP of 0.99%, 0.13%, and 2.46%, respectively [51]. Moreover, Rajavelu et al. [53] also presented a method for carbon measurement of raw coal by combining the atomic carbon, molecular carbon, and emission from other inorganic elements. The temporal  $C_2$  emission data were then added to improve the analysis accuracy; RMSEP and RSD are reduced from 10.8% to 4.1% and from 11% to 6.0%, respectively.

The contents of moisture and volatile fractions, which vary with the environment, are important essential characteristic indicators of coal and could affect the laser-coal interaction. Chen et al. [54] performed a LIBS study on coal samples with different moisture contents varying from 1.2% to 22%. The study demonstrated that moisture evaporated earlier than other components of coal and then pushed to the upper layer of the plasma, which contributed to stronger atomic H emission at the plasma front. Yao et al. [55] investigated the effects of volatile content variation, and the matrix changed from coal to char when LIBS detection was conducted. The results showed that the volatile matter is easily affected by the thermal effect of high-temperature plasma, leading to more matter vaporized in coal samples with high volatility. The laser energy was consumed and shielded by the volatile matter, thereby leading to less efficient vaporization and atomization of the mineral elements (Si, Al, and Ca) and hence lowering their emission intensities. Furthermore, we carried out temporally and spatially resolved LIBS to investigate the mechanism of volatile matter from coal plasma in an argon atmosphere. The results indicated that volatile matter would result in a diverse plasma morphology and parameter distribution at a later stage of plasma [56].

Although, at present, the effects of all the major properties of coal on LIBS signals have not been fully clarified, quantitative analysis results of different types of coal samples have been improved [57,58]. If the coal samples are first classified according to specific parameters or criteria like volatile matter and ash, the classify-then-analyze approach could be extended to other solid energy materials. Systematic fundamental studies on LIBS analysis of energy materials are ongoing. The goal of fundamental research is to understand the influence of the sample properties on the LIBS signal. Thus, it is critical to develop a matrix effect correction method and then to create a robust evaluation method combined with the development of an information database on the

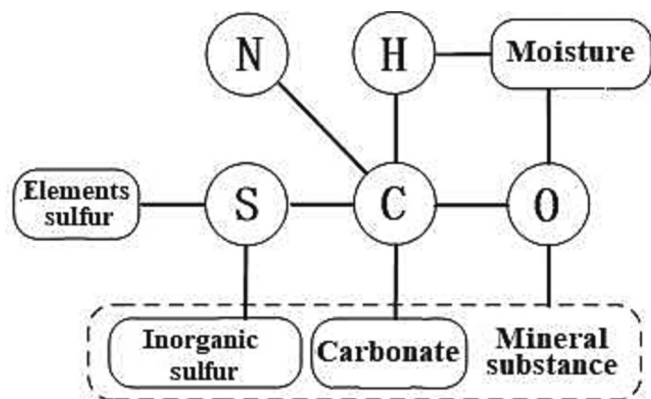


Fig. 3. Schematic diagram of the main non-metallic elements in solid fuels.

organic-containing materials and the environment influences, for example carbon molecular emissions [45–50]. Fig. 4 shows the representative carbon-related emissions from a typical coal sample plasma, where molecular  $C_2$  emission from the Swan system ( $d^3\Pi_g \rightarrow a^3\Pi_u$ ) and CN from the violet system ( $B^2\Sigma^+ \rightarrow X^2\Sigma^+$ ) are commonly obtained together with atomic carbon emission.

The temporal evolution of atomic and molecular carbon emissions from a coal sample under different ambient gases (air, argon, and helium) was reported in our previous work [52]. The rotational temperature

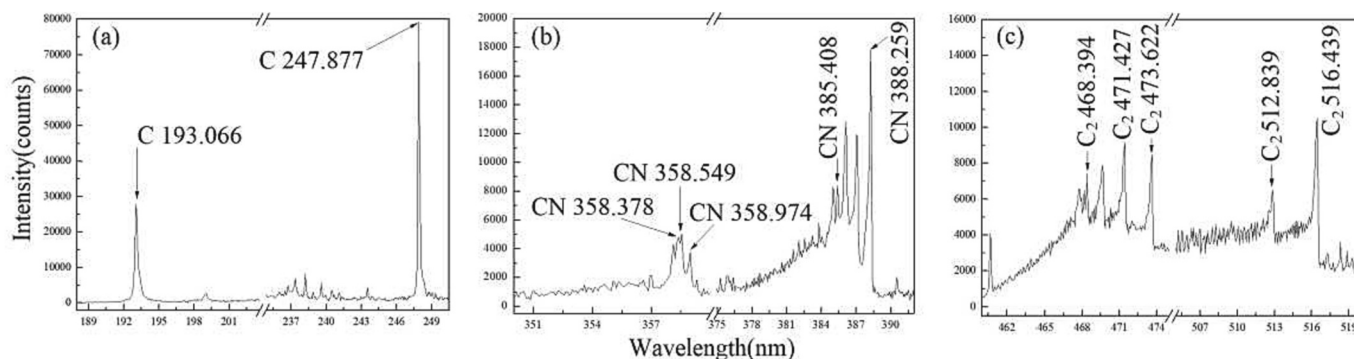


Fig. 4. Typical LIBS spectra from the coal sample: (a) atomic carbon, (b) molecular CN, and (c) molecular C<sub>2</sub> [51].

quality of energy materials.

### 2.3. Analysis of the properties of solid energy materials

LIBS is a promising technology for fuel properties analysis with a large potential market in the energy industry, for example, coal production and utilization, and biomass and petroleum industries. In recent years, the application of LIBS to classify the type of coal led to the development of equipment and methods. Overall, taking coal as the starting point, a framework and review of strategy and a roadmap for solid fuel analysis are summarized and recommended in this section.

#### 2.3.1. Rock mineral

In industrial processes, the coal on a conveyor belt is in the form of rock mineral. Several LIBS devices have been developed and installed on the conveyor belt for online measurements. Gaft et al. [59,60] developed a LIBS instrument with  $150 \times 80 \times 130 \text{ cm}^3$ , 250 kg weight (as shown in Fig. 5), for the measurement of different ores. An ultrasonic height sensor was employed to adjust the optical focus based on the height of the rock on the moving belt. Five laboratory samples with ash content varying from 12.5 to 53.9% were utilized to calibrate the system with water-influence correction. The LIBS device was evaluated for its performance for on-belt operations by measuring the ash content of coal at Optimum Colliery. The results were compared with an existing online PGNA instrument and with routine analyses in an analytical laboratory. The trial was carried out over a period of four months. The best-fit linear regression line between the PGNA and LIBS result was characterized by  $R^2 = 0.72$  and  $SD = 0.73$ . Romero et al. [61,62] not only established a laboratory LIBS system to measure slagging propensity but also proposed an online system assembled for a full-scale, over-the-belt installation at a coal-fired power plant, as described in Fig. 6. The ancillary optics components provided enough depth of field to



Fig. 5. Online LIBS system (LDS) on a moving belt conveyor developed by Gaft et al. [60].



Fig. 6. Schematic of an online LIBS system developed by Romero et al. [62].

compensate for significant changes in the height of the moving coal layer. The system worked for seventy-three hours with an emphasis on the detection of iron, which was verified by analyzing the reference coal sample with the conventional method, with a relative measurement accuracy of 6.7% (1.07% absolute).

As LIBS is a point-measurement technology, it is important to overcome the influence of distance change between the laser focus and the sample surface. A variable focal length optical system or a mechanical system can be used to keep the collection optics at a constant distance from the sample. Alternatively, a mirror-based optical system with a sufficiently large depth of field [63,64] can also be used. However, there is still a lack of a stable standardized method that is universally applicable in all situations. In addition, serious matrix effects arising from the influence of surface moisture and impurities as well as differences in physical and chemical properties of the energy materials would affect the laser-material interaction and hence spectral emissions. For example, when the laser hits a pocket of water inclusion, low-quality spectra unsuitable for LIBS evaluation are produced. These spectra could lead to serious analysis errors. With existing data-analysis methods, each spectrum is analyzed for its quality on whether it contains adequate information; if not, the spectrum needs to be discarded. However, this procedure of spectrum filtering is not without a blind spot, and spectrum that is only partially affected may remain unnoticed and uncorrected. Furthermore, the sample surface may not represent the bulk average because the internal compositions of ores are sometimes inhomogeneous. The surface-analysis nature of LIBS is not necessarily an advantage in this case. Certainly, there are other issues for coal analysis, in particular for a system to be operated outdoors under real environmental conditions with dust, rain, extreme temperatures, and mechanical vibrations. For example, sealed panels, shock absorbers, and air conditioning are necessary. Therefore, future work should include solutions or better optimization methods to solve the aforementioned issues for raw mineral energy materials analysis with LIBS.

### 2.3.2. Pellet samples

As mentioned above, raw coal is a sedimentary rock with heterogeneous composition, diverse shape, and complex physicochemical properties upon which the laser–material interaction depends. Subsequently, multiple sources of uncertainty exist in the plasma and its spectral emission. Thus, for accurate results, the plasma signal needs to be measured in a stable environment with a well-defined procedure. For example, raw coal mineral would be crushed, sieved, processed prior to the analysis, and pressed into pellets for a flat, rigid, and relatively homogeneous surface. To maintain a relatively stable laser interaction process, particle size parameters [65] and pressure for pellet pressing and binder were optimized. The collection optics could easily match the plasma plume position for optimized collection efficiency [66,67]. Furthermore, based on sample conditions, researchers have reported parametric optimization on laser parameters [68–70], optical configuration [43,69], and environmental conditions [44,52].

With the development of data-mining algorithms and artificial intelligence, most quantitative analyses nowadays are performed with chemometrics, machine learning, and various spectral data preprocessing methods. Application of LIBS for coal analysis is mainly promoted by continuous development in mathematical, statistical modeling, and equipment hardware. They can provide intelligent optimization, data extraction, and automated correction for the spectral signal. In 2018, Wang et al. [36] summarized the process details of quantitative analysis of coal, including data pretreatment (e.g., signal accumulation and averaging, data filtering, normalization, and spectrum standardization) and classification model (e.g., univariate calibration, multivariate calibration, and calibration-free methods). On this basis, in addition to a review of the literature from 2018 to the present, the reported data preprocessing, modeling, and results of quantitative analysis of coal are listed in Table 2. Abbreviation details are all listed in Table 3.

In addition to coal, biomass is a commonly used solid fuel that is mainly retrieved from agriculture and forestry by-products, bamboo, and wood processing waste. It is considered as a source of clean energy because of its renewability [40]. Recently, the use of LIBS for biomass analysis has attracted increasing attention. The performance of LIBS has demonstrated the potential for industrial application in timely monitoring of biomass fuel qualities [37,38,109,110]. For heat and electricity utilization, biomass is usually pressed into pellets. The matrix effects of the pelletizing conditions (e.g., pelletizing pressure and temperature, its moisture content, and particle size) on the spectral quality were investigated, and spectral pretreatment and modeling methods were proposed [111]. The research that was conducted on coal quality analysis was well extended to biomass detection. It is worthy of mentioning that the source of biomass fuels is complex; it faces additional serious matrix differences compared to coal due to the diverse types as well as production and transportation processes. The reliability and extensiveness of the utilization of LIBS in biomass needs further improvement.

Until now, the better scheme is to take the online produced pellet as the measurement sample, which gives higher representativeness and more stable LIBS signals and thus a higher-quality analysis. However, the processes of operation and control for the sample collection and loopback need several mechanical devices. In the energy industry market, companies have launched highly automated LIBS instruments for different energy materials. In this context, common automation includes sample pretreatment, measurement, and return after testing. Commonly, the LIBS device is mounted beside the main conveyor belts for coal sampling. The samples then are subjected to a series of preprocessing, such as grinding (if required), mixing, and pressing into pellets and finally are returned back to the belt to save fuel and to not generate waste.

### 2.3.3. Pulverized particle sample

The purpose of LIBS measurement is to characterize the properties of input material of an industrial process, where a range of particle morphology and the state of gas-solid two-phase flow exist. For thermal

**Table 2**  
Analytical results of coal properties for the coal pellet samples.

Spectral pretreatment & calibration method	Validation set results	Reference
PLS using data uncertainty	Ash: RMSEP = 1.15%, AAE = 0.91%, $R^2 = 0.98$ . Calorific value: RMSEP = 0.09%, MSE = 0.09, $R^2 = 0.99$ ; Ash: RMSEP = 0.25%, MSE = 0.06, $R^2 = 0.99$ ;	[71]
PCR	Volatile: RMSEP = 0.69%, MSE = 0.44, $R^2 = 0.99$ ; Fixed carbon: RMSEP = 0.66%, MSE = 0.41, $R^2 = 0.99$ ; Moisture: RMSEP = 0.25%, MSE = 0.06, $R^2 = 0.99$ .	[72]
ANN	Volatile: $R^2 = 0.99$ .	[73]
Adaptive subset matching (ASM) & PLSR	Calorific value: RMSEP = 0.62 MJ/kg, RSD = 2.7%, $R^2 = 0.98$ . Ash: RMSEP = 1.84%, $R^2 = 0.82$ ; Volatile: RMSEP = 1.09%, $R^2 = 0.98$ ;	[74]
Histogram of oriented gradient (HOG) and k-means & PLSR	Calorific value: RMSEP = 0.84 MJ/kg, $R^2 = 0.83$ .	[75]
Ensemble variable selection (least absolute shrinkage and selection operator (LASSO) & competitive adaptive reweighted sampling (CARS) & recursive weighted partial least squares (rPLS) & PLS	Fixed carbon: RMSEP = 1.17%; Volatile: RMSEP = 0.95%; Ash: RMSEP = 1.76%;	[76]
WTD, distance correlation (DC) and recursive feature elimination with cross-validation (RFECV) & SVR	Calorific value: RMSEP = 0.84 MJ/kg.	[77]
ANN	Calorific value: RMSEP = 0.58 MJ/kg, RSD = 0.22%, ARE = 2.27%, $R^2 = 0.99$ . Calorific value: RMSEP = 0.69 MJ/kg, RSD = 0.22%, AAE = 0.56 MJ/kg; Ash: RMSEP = 1.09%, RSD = 2.2%, AAE = 0.69%; Volatile: RMSEP = 1.12%, RSD = 1.4%, AAE = 0.87%.	[78]
WTD & SVR (calorific value and ash)	Calorific value: RMSEP = 0.80 MJ/kg, RSD = 0.26 MJ/kg, ARE = 1.82%, AAE = 0.47 MJ/kg, $R^2 = 0.99$ ;	[79]
WTD & PLSR (volatile)	Ash: RMSEP = 0.60%, RSD = 0.57%, ARE = 2.99%, AAE = 0.55%, $R^2 = 0.99$ ; Volatile: RMSEP = 0.76%, RSD = 0.79%, ARE = 3.63%, AAE = 0.67%, $R^2 = 0.99$ .	[79]
Classification (SVM and GA) & PLSR	Calorific value: RMSEP = 0.41 MJ/kg, $R^2 = 0.99$ ; Ash: RMSEP = 0.91%, $R^2 = 0.99$ ; Volatile: RMSEP = 0.77%, $R^2 = 0.99$ .	[57]
Classification (SVM) & PLSR	Calorific value: RMSEP = 1.08 MJ/kg, ARE = 3.93%, $R^2 = 0.97$ . Calorific value: RMSEP = 0.70 MJ/kg, $R = 0.99$ ;	[58]
PSO&K-ELM	Ash: RMSEP = 1.90%, $R = 0.99$ ; Volatile: RMSEP = 1.09%, $R = 0.99$ .	[80]
Multipoint smoothing and second-order derivation & PLS	Calorific value: RMSEP = 0.28 MJkg <sup>-1</sup> , $R = 0.99$ .	[81]
PCA & PLS	Volatile: $R^2 = 0.99$ , RMSEP = 0.66%, ARE = 1.96%.	[82]
WTD and PCA & WNN	$R^2 > 0.93$ and RMSE < 0.26 for 7 Ash related oxides. Measurement errors: Calorific value: 0.07 MJ/kg;	[83]
Spectrum standardization and identification & dominant factor PLSR	Ash: 0.07% (<15% range); 0.17% (15–30% range); 0.23% (>30% range); Volatile: 0.03% (<20% range), 0.11% (20–40% range).	[84]

(continued on next page)

Table 2 (continued)

Spectral pretreatment & calibration method	Validation set results	Reference
PCA & SVM	Ash: Measurement accuracy = 0.31%, $R = 0.99$ , AAE = 2.36%. Calorific value: RMSEP = 0.85 MJ/kg, $R^2 = 0.91$ , ARE = 3.68%, AAE = 0.65%;	[69]
PCA & SVR	Ash: RMSEP = 1.82%, $R^2 = 0.96$ , ARE = 5.48%, AAE = 1.77% (>30% range); 1.37 (<30% range); Volatile: RMSEP = 1.69%, $R^2 = 0.95$ , ARE = 4.42%, AAE = 1.02% (>20% range), 1.11% (<20% range). Calorific value, RMSEP = 1.33 MJ kg <sup>-1</sup> , ARE = 2.71%, $R^2 = 0.97$ ;	[85]
Dominant factor based PLS (calorific value, volatile and ash)	Volatile, RMSEP = 1.41%, ARE = 5.47%, $R^2 = 0.97$ ;	[86]
conventional PLS model (moisture)	Ash, RMSEP = 3.49%, ARE = 12%, $R^2 = 0.93$ ;	
Multivariate model	Moisture: RMSEP = 0.87%, ARE = 26.2%, $R^2 = 0.97$ . Ash: $R = 99\%$	[87]
PCR	Volatile: $R = 0.991$ , AAE = 1.13%, ARE = 4.54%.	[88]
PLS	Ash: $R = 0.97$ .	[89]
PLS	Carbon: RMSEP = 4.1%, RSD = 6%, $R^2 = 0.82$ . Carbon: RMSEP = 1.59%, RSD = 2.5%, $R^2 = 0.98$ ;	[53]
Classification (adaptive subset matching (ASM)) & PLSR	Hydrogen: RMSEP = 0.10%, RSD = 4.3%, $R^2 = 0.98$ ;	[74]
	Nitrogen: RMSEP = 0.07%, RSD = 6.6%, $R^2 = 0.94$ .	
Ensemble variable selection (least absolute shrinkage and selection operator (LASSO) & competitive adaptive reweighted sampling (CARS) & recursive weighted partial least squares (rPLS)) & PLS	Sulfur: RMSEP = 0.12%.	[76]
Internal reference self-absorption correction (IRSAC) and the density correction & calibration-free LIBS (CF-LIBS)	Carbon: ARE < 1%.	[90]
Normalization over the whole spectral area & SVR	Carbon: RMSEP = 1.08%, RSD = 0.47%, ARE = 1.39%, AAE = 0.94%, $R^2 = 0.99$ ;	[79]
	Hydrogen: RMSEP = 0.21%, RSD = 0.08%, ARE = 1.39%, AAE = 0.19%, $R^2 = 0.98$ . Carbon: $R^2 = 0.67$ , RMSEC = 5.71%, RMSEV = 4.84%, RSD = 2.8% (Air);	
PLSR	$R^2 = 0.58$ , RMSEC = 5.82%, RMSEV = 4.21%, RSD = 4.6% (N <sub>2</sub> ); $R^2 = 0.85$ , RMSEC = 5.57%, RMSEV = 4.22%, RSD = 3.9% (Ar). Nitrogen: $R^2 = 0.98$ , RMSEP = 2.08%;	[91]
SPA & PLS	Sulfur: $R^2 = 0.95$ , RMSEP = 20.82%.	[92]
Univariate calibration (DP-LIBS)	Sulfur: RMSECV = 0.14%, $R^2 = 0.99$ , LOD = 0.04% (He).	[93]
MLR & SVR (correct the residue errors)	Carbon: RMSEP = 1.43; $R^2 = 0.99$ .	[51]
Internal reference line self absorption correction & calibration-free LIBS (CF-LIBS)	Carbon: ARE = 3.32%, RSD < 5%.	[94]
Univariate model	Carbon: $R^2 = 0.98$ .	[67]
K-ELM	Sulfur: $R^2 = 0.98$ , RMSE = 0.77 wt%.	[95]

Table 2 (continued)

Spectral pretreatment & calibration method	Validation set results	Reference
PCA & PLS	Carbon: $R^2 = 0.99$ , RMSEP = 0.68%, ARE = 1.17%	[82]
Spectrum standardization and identification & dominant factor PLSR	Measurement errors: Carbon: 0.42%; Hydrogen: 0.05%.	[84]
Spectrum standardization & dominant factor based PLSR (spatial confinement)	Carbon: RMSEP = 1.35%, $R^2 = 0.99$ , ARE = 1.66%, AAE = 1.08%.	[96]
PLS	Carbon: RMSEP = 1.55%, $R^2 = 0.99$ (1064 nm laser); RMSEP = 1.64%, $R^2 = 0.99$ (266 nm laser).	[70]
Dominant factor based PLS	Carbon: RMSEP = 1.51%, $R^2 = 0.99$ . Carbon: RMSEP = 1.94%, $R^2 = 0.98$ , ARE = 1.67% (He); RMSEP = 2.67%, $R^2 = 0.99$ , ARE = 1.71% (Ar);	[97]
WTD & PLS	RMSEP = 3.44%, $R^2 = 0.99$ , ARE = 1.88% (Air).	[98]
Spectrum standardization & dominant factor based PLSR	Carbon: RMSEP = 1.63%, ARE = 1.82%, $R^2 = 0.99$ . Carbon: RMSEP = 4.25%, ARE = 4.96%, $R^2 = 0.87$ , RSD = 9.8% (Air); RMSEP = 3.32%, ARE = 2.81%, $R^2 = 0.96$ , RSD = 13% (He); RMSEP = 3.49%, ARE = 2.98%, $R^2 = 0.95$ , RSD = 8.5% (Ar);	[99]
PLS	Hydrogen: RMSEP = 0.48%, ARE = 6.69%, $R^2 = 0.82$ , RSD = 6.8% (Air); RMSEP = 0.27%, ARE = 4.56%, $R^2 = 0.91$ , RSD = 9.8% (He); RMSEP = 0.24%, ARE = 2.78%, $R^2 = 0.98$ , RSD = 6.2% (Ar).	[44]
Internal calibration & univariate model	Carbon: RMSEP = 6.25%, ARE = 10.14%, $R^2 = 0.76$ . Sulfur: SD = 0.11, $R^2 = 0.88$ , ARE = 7.5%.	[100]
Univariate model (DP-LIBS)	Sulfur: $R^2 = 0.99$ .	[101]
Univariate model (DP-LIBS)	Sulfur: $R^2 = 0.99$ .	[102]
Optimal analytical line selection, internal normalization and temperature correction & multi-line analysis	Organic oxygen (anthracite coal): accuracy of 1.15–1.37%, ARE = 19.39%.	[41]
Spectral normalization & univariate model	Al: RMSE = 6.7%, $R^2 = 0.99$ ; Si: RMSE = 9.97%, $R^2 = 0.98$ ; Ca: RMSE = 2.8%, $R^2 = 0.98$ ; Fe: RMSE = 16.3%, $R^2 = 0.96$ ; Mg: RMSE = 6.1%, $R^2 = 0.99$ .	[103]
Internal reference self-absorption correction (IRSAC) & calibration-free LIBS (CF-LIBS)	Ca, Si, Fe, Ti, Mg, Na, K, Li, Al: ARE < 10%, RSD < 5%.	[94]
	Ca: $R = 0.99$ , LOD = 0.01%, RSD = 8.2%, ARE = 7.30%; Mg: $R = 0.98$ , LOD = 0.02%, RSD = 6.4%, ARE = 5.80%;	
'Bode Rule/DC Level' normalization and spectral data screening & univariate model	Al: $R = 0.96$ , LOD = 0.02%, RSD = 5.2%, ARE = 6.17%; Fe: $R = 0.97$ , LOD = 0.02%, RSD = 7.8%, ARE = 4.40%; Si: $R = 0.97$ , LOD = 0.08%, RSD = 5.8%, ARE = 5.12%.	[104]
Univariate model	Mg: $R^2 = 0.99$ ; Ca: $R^2 = 0.98$ .	[43]
Univariate model	Al: $R = 0.98$ , RSD = 8.6%; Ca: $R = 0.99$ , RSD = 5.0%; Fe: $R = 0.99$ , RSD = 8.6%; Mg: $R = 0.98$ , RSD = 12%; Si: $R = 0.99$ , RSD = 3.9%.	[68]
Normalization, spectral data screening and spectral	Al: ARE = 5.93%, RSD = 5.9%; Ca: ARE = 16.52%, RSD = 20%; Fe: ARE = 7.86%, RSD = 3.9%;	[105]

(continued on next page)

Table 2 (continued)

Spectral pretreatment & calibration method	Validation set results	Reference
deconvolution & univariate model	K: ARE = 7.59%, RSD = 11%; Mg: ARE = 11.18%, RSD = 11%; Si: ARE = 3.60%, RSD = 2.4%; Na: ARE = 18.82%, RSD = 25%; Ti: ARE = 11.43%, RSD = 7.7%. Mg: R = 0.91, LOD = 200 ppm; Na: R = 0.98, LOD = 70 ppm; Ca: R = 0.91, LOD = 60 ppm; Fe: R = 0.91, LOD = 90 ppm; Al: R = 0.99, LOD = 60 ppm; Si: R = 0.93, LOD = 200 ppm. Softening temperature: RMSECV = 4.88 °C, RMSEP = 8.15 °C, R <sup>2</sup> = 0.99;	[106]
Univariate model	Hemisphere temperature: RMSECV = 9.11 °C, RMSEP = 11.3 °C, R <sup>2</sup> = 0.99. Initial deformation ash fusion temperature: RMSEP = 56 °C, measurement reproducibility = ±14 °C	[107]
Classification (SVM) & SVR		[108]
ANN		

Table 3  
Abbreviations of analytical methods and indicators.

Abbreviation of methods	Full name	Abbreviation of indicators	Full name
ANN	Artificial Neural Network	RMSE	Root Mean Square Error
AAE	Average Absolute Error	RMSEP	Root Mean Square Error of Prediction
ARE	Average Relative Error	RMSEC	Root Mean Square Error of Calibration
GA	Genetic Algorithm	RMSEV	Root Mean Square Error of Validation
K-ELM	Kernel Extreme Learning Machine	RMSECV	Root Mean Square Error of Cross Validation
LOD	Limit of Detection	RSD	Relative Standard Deviation
MLR	Multiple Linear Regression	SVR	Support Vector Regression
PLS	Partial Least Square	SVM	Support Vector Machine
PLSR	Partial Least Square Regression	SPA	Successive Projections Algorithm
PSO	Particle Swarm Optimization	WTD	Wavelet Threshold De-noising
PCR	Principal Component Regression	WNN	Wavelet Neural Network
R <sup>2</sup>	Coefficient of Determination	/	/
R	Correlation coefficient	/	/

power plants, pulverized coal enters the furnace mainly in the form of a gas-solid flow [112] and can be sampled from the transmission pipes before entering the furnace. Because LIBS directly analyzes the flow of coal particles, it simplifies significantly the sample detection process and reduces the measurement time. Moreover, the measurement results directly reflect the fuel characteristics in the furnace and provide the benefit of real-time combustion control. By contrast, it would take more than four hours for the raw fuel on the belt to turn into pulverized coal and enter the furnace. As such, LIBS is appropriate for continuous on-site monitoring of coal properties.

In the early 1980s, Loree et al. [113] applied LIBS for the detection of atomic constituents of gases and gas-entrained particulates in different

field conditions. For the coal gasifier product stream in hostile environments, the detection includes Be in the form of powdered BeF<sub>2</sub> in free air and P, S, and Cl in the samples prepared by filling a cell with the background gas and vapor. Subsequently, Ottesen et al. [114] proposed the use of LIBS for semi-quantitative measurements of Mg, Ca, Al, Si, Fe, and Ti in different coal particles entrained by a vertically flowing column of gases from a premixed flat-flame burner of circular symmetry. Subsequently, it was applied to a practical coal-fired flow facility (CFFF) at the University of Tennessee Space Institute (UTSI)'s magnetohydrodynamics (MHD) test facility in the 1995s [115]. The spectral intensity in different observational directions was investigated to evaluate the most suitable configuration for large-scale applications. Accordingly, it has successfully achieved simultaneous measurements of multiple elements (Ca, Fe, Al, Ti, and Sr) in a harsh, turbulent, and highly luminous combustion environment.

Our research group is committed to the direct detection of coal particle flow by using LIBS and has carried out multiple systematic research works (e.g., spectral data preprocessing methods [116], quantitative analysis methods [117], and detecting system design [118]). The developed prototype LIBS device for the detection of particle flow samples is shown in Fig. 7a, including sampling, measuring, and returning systems. A gas/solid system is established to produce particle flow for direct LIBS analysis. The system of producing particle flow contains an ejector, cyclone separator, measuring chamber, pipes, and the other accessories (Fig. 7c). The developed software operating interface is shown in Fig. 7b. The mechanical complexity of the overall system is simple, although interpretation of the measurement data could be challenging.

When applying LIBS for direct particle-flow detection, because the breakdown of some particles is not fully but only partially complete, some acquired spectra do not contain emission lines of the most significant elements. The partial-breakdown spectra are not considered analytically useful [116,117]. As such, schemes are proposed to identify representative spectra and reject those from partial breakdown, including the signal-to-noise ratio (SNR) method, the absolute intensity method, and standard deviation (SD) [116]. Recently, we proposed an image information-assisted screening method for particle flow spectral data identification to improve the LIBS quantitative measurement on variable coal particle flow. It exhibits superior analytical performance compared with SD and the SNR method [118]. Fig. 8 shows typical plasma images of three excitation scenarios (effective breakdown, partial breakdown, and invalid breakdown) and the corresponding spectra for the coal particle flow. The brightness of the central part of the plasma images is an effective indicator for data screening. As depicted in Fig. 8, a relationship between the plasma area and the spectrum exists.

The hardware for laser focusing specifically designed and optimized for coal particle analysis was reported. For example, Yao et al. [119] proposed the use of tapered tubes with different diameters for the coal particle flow for laser ablation, as shown in Fig. 9. The results showed that the tube with a diameter of 5.5 mm was suitable to enrich the coal particles for beam-focusing and subsequently to obtain further strong effective spectra. On this basis, they developed a rapid coal particle flow analyzer based on LIBS, which included a pulverized coal feeding module, a spectral measurement module, and a control module, as shown in Fig. 10. After the identification of the valid data and the spectral correction, the quantitative analysis of ash, volatile matter, fixed carbon, and gross calorific value of coal was done with, respectively, average absolute errors of 0.82%, 0.85%, 0.96%, and 0.48 MJ/kg, which offer similar accuracy levels compared to PGNA [120]. In their subsequent works, they focused on enhancing and stabilizing the plasma for direct analysis of particle flow [121] and optimization of the focusing system by using dual lenses [122].

There is a correlation between particle composition and diameter in actual industrial processes. In the laboratory, the experimental objects (coal particles) have been ground and screened with a certain diameter range. During the grinding process, some of the mineral matter is



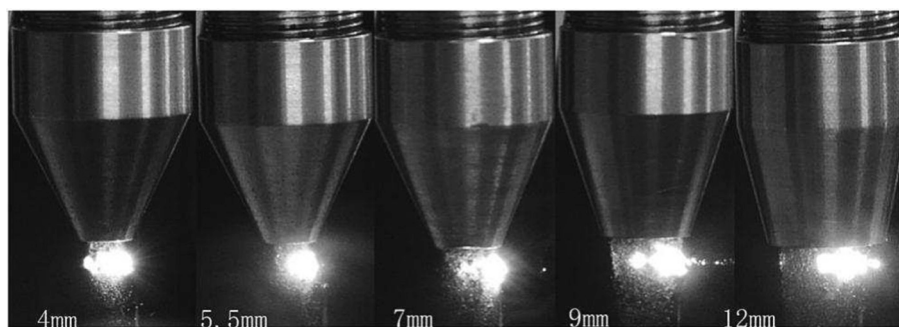


Fig. 9. A set of tapered tubes with different diameters to produce coal particle flow for laser ablation (the laser strikes horizontally from the right, and the bright parts are plasmas) [119].

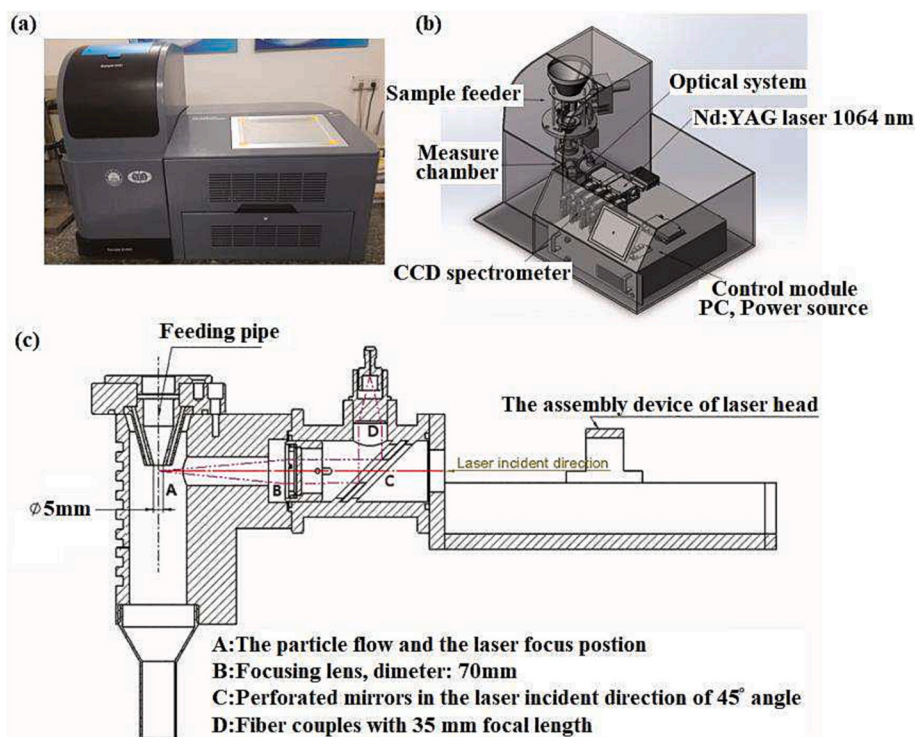


Fig. 10. A rapid coal particle flow analyzer: (a) appearance, (b) schematic composition, and (c) sectional view of the LIBS equipment [120].

performance in particle flow detection [122] was comparable to that of analysis on the form of pellet or solid. The generation and signal collection of plasma in gas-solid flow is a complex process involving particle ablation under the influence of gas and mixing. A more in-depth understanding of the process interaction between the laser and particle flow would be a basis for designing satisfactory improved methods.

### 3. Spontaneous emission and LIBS for combustion diagnostics

Fuel combustion usually undergoes a series of complex, inter-related physical and chemical processes, including chemical reactions, fluid flow, and heat and mass transfer. The combustion flame is the most direct reflection of the combustion state. However, conventional flame detection technology (e.g., thermocouple) presents major limitations in practical applications due to its single function. With an in-depth understanding of the characteristics of combustion flame and the emergence of new industrial technology, optical-based methods of flame detection have also developed rapidly. At present, the main combustion diagnostics are image monitoring and laser spectroscopy. This section reviews the application of atomic spectroscopy in combustion

diagnostics, including spontaneous emission spectroscopy (Section 3.1) and LIBS (Section 3.2).

#### 3.1. Spontaneous emission for combustion diagnostics

##### 3.1.1. General

Spontaneous emission is a common method of combustion diagnostics. During the combustion process, fractions of atoms, molecules, and free radicals in the flame are in their excited states. When these excited states undergo radiative decay to their ground state or a lower energy level, a photon corresponding to the energy difference between the upper and lower energy levels is emitted. The spontaneous emission spectrum is closely related to the characteristic parameters (e.g., temperature distribution and structure of the flame). It can be readily measured by a spectrometer or an imaging device and can be applied in severe detection conditions. A series of investigations have been conducted on the measurements of temperature (Section 3.1.2), free radicals (Section 3.1.3), and the release of alkali metals (Section 3.1.4) from a combustion flame.

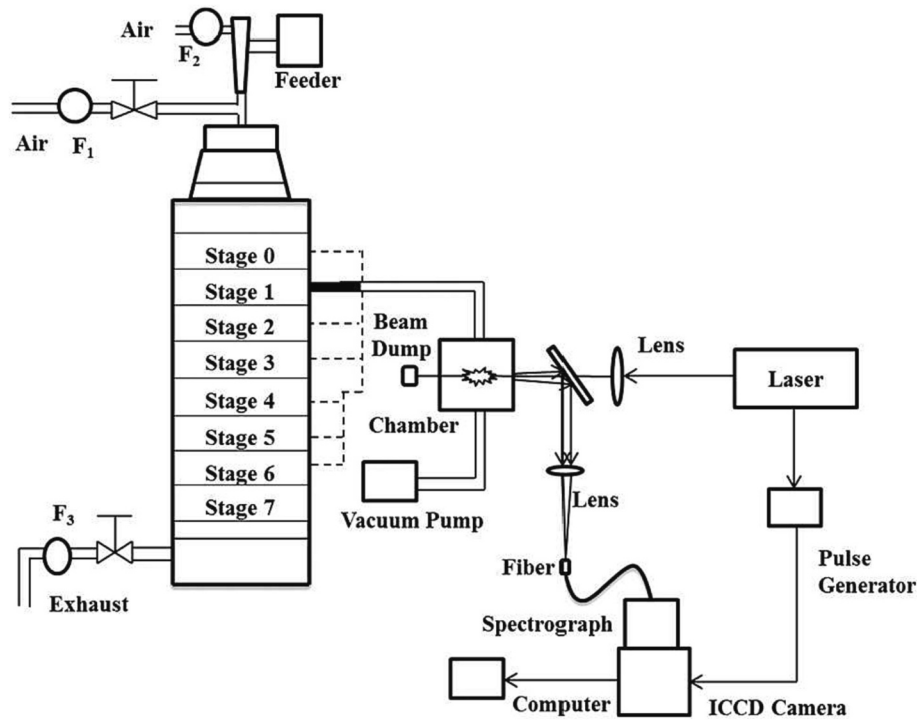


Fig. 11. The size-segregated particles system for LIBS measurement [124].

### 3.1.2. Temperature measurement

Temperature is the most important parameter in combustion diagnostics. It directly relates to combustion efficiency [126], degree of fuel burnout [127], flame stability [128], and pollutant generation [129], and thus is the basis of combustion mechanism research [130,131]. There are various well-established or emerging methods for flame temperature measurement. These methods can be further divided into two categories: contact and non-contact measurements. The former, for example through thermocouple or thermistor, has a limitation on the upper measurable temperature and is invasive on the combustion field [132,133]. For the latter, optical detection schemes have been developed to effectively overcome the shortcomings of contact measurement techniques. Among them, radiative emission has been widely applied as a simple and effective method in flame temperature measurement.

The basic principle of temperature measurement based on radiative emission is based on Planck's law, which describes the spectral intensity distribution of blackbody radiation:

$$I_b(\lambda, T) = C_1 \lambda^{-5} \frac{1}{\exp\left(\frac{C_2}{\lambda T}\right) - 1} \quad (1)$$

where  $I_b(\lambda, T)$  is the monochromatic radiation intensity of an absolute blackbody in  $W/m^3$ ,  $\lambda$  stands for the wavelength in m,  $T$  stands for the thermodynamic temperature in K,  $C_1$  and  $C_2$  are respectively called first and second radiation constants, with  $C_1 = 3.742 \times 10^{-16} W \cdot m^2$  and  $C_2 = 1.4388 \times 10^{-2} m \cdot K$ . For an actual object with an emissivity  $\epsilon(\lambda)$ , its monochromatic radiation intensity is:

$$I(\lambda, T) = \epsilon(\lambda) C_1 \lambda^{-5} \frac{1}{\exp\left(\frac{C_2}{\lambda T}\right) - 1} \quad (2)$$

If the product of wavelength  $\lambda$  and temperature  $T$  is far less than the second radiation constant  $C_2$  (this condition is satisfied if the temperature is between 800 K and 2000 K and wavelength ranges from 300 nm to 1000 nm [134], which applies to the most practical application), Formula (2) is simplified to the Wien's radiation law:

$$I(\lambda, T) = \epsilon(\lambda) \frac{C_1}{\lambda^5} \exp\left(-\frac{C_2}{\lambda T}\right) = \epsilon(\lambda) I_b(\lambda, T) \quad (3)$$

The above formula describes the relationship between radiation intensity and temperature, and the unknowns are only temperature and emissivity. Therefore, a suitable emissivity model (for example, the gray emissivity or the Hottel-Broughton emissivity model) is selected to solve the temperature. It is worthy to mention that the temperature measurement method based on the Planck equation is applicable only to a flame containing solid particles or soot, the radiation of which is really close to that of a blackbody. Otherwise, plasma radiation is very far from blackbody radiation.

Based on the detection device, emission radiation thermometry is further divided into two categories: imaging and spectroscopy. Image thermometry is usually grouped into monochrome thermometry, two-color thermometry, and multi-color thermometry. It is generally necessary to install a filter with a specific wavelength or band to assist the detection. In monochrome thermometry, the flame temperature of a specific location is first measured by a thermocouple or a pyrometer to set up a reference, and subsequently, the temperature distribution in two or three dimensions is determined using the radiation images according to the formula [135]:

$$\frac{I(x, y)}{I(x_0, y_0)} = \exp\left[-\frac{C_2}{\lambda} \left(\frac{1}{T(x, y)} - \frac{1}{T(x_0, y_0)}\right)\right] \quad (4)$$

where  $(x_0, y_0)$  is the coordinate of the reference point,  $(x, y)$  is the coordinate of the other spatial locations in the image, and  $\lambda$  is the wavelength from the filter parameters. From the above equation,  $T(x, y)$  can be solved as:

$$T(x, y) = \frac{1}{\frac{1}{T(x_0, y_0)} - \frac{\lambda}{C_2} \ln \frac{I(x, y)}{I(x_0, y_0)}} \quad (5)$$

The application of the monochrome thermometry method is limited due to the need for a reference-temperature measurement. By contrast, a reference is not required in two-color or multi-color thermometry, whose principles are as follows [136]:

$$\frac{I_R}{I_G} = \frac{\int_{\lambda_s}^{\lambda_e} \left[ \varepsilon(\lambda) \eta_R(\lambda) \frac{C_1 \lambda^{-5}}{\exp(C_2/\lambda T)} \right] d\lambda}{\int_{\lambda_s}^{\lambda_e} \left[ \varepsilon(\lambda) \eta_G(\lambda) \frac{C_1 \lambda^{-5}}{\exp(C_2/\lambda T)} \right] d\lambda} \quad (6)$$

where subscript *R* and *G* stand for red band and green band, respectively;  $\lambda_s$  and  $\lambda_e$  are the starting and ending wavelengths of the corresponding wavelengths of the image detector in m, respectively, which can be obtained according to filter parameters;  $\eta(\lambda)$  is the experimentally calibrated response efficiency of the image detector channel. The Hottel and Broughton emissivity model or other assumed emissivity models are usually used to acquire the emissivity characteristics of the flame.

Based on the integral median theorem, it is obtained that:

$$\frac{I_R}{I_G} = \frac{\varepsilon(\lambda_\alpha) \eta_R(\lambda_\alpha) \frac{C_1 \lambda_\alpha^{-5}}{\exp(C_2/\lambda_\alpha T)}}{\varepsilon(\lambda_\beta) \eta_G(\lambda_\beta) \frac{C_1 \lambda_\beta^{-5}}{\exp(C_2/\lambda_\beta T)}} \quad (7)$$

where  $\alpha$  and  $\beta$  are derived from the integral median theorem; then colorimetric thermometry can be described as:

$$T = \frac{C_2 \left( \frac{1}{\lambda_\beta} - \frac{1}{\lambda_\alpha} \right)}{\ln \frac{I_R}{I_G} - \ln \frac{\eta_R(\lambda_\alpha)}{\eta_G(\lambda_\beta)} - 5 \ln \frac{\lambda_\beta}{\lambda_\alpha} - \ln \frac{\varepsilon(\lambda_\alpha)}{\varepsilon(\lambda_\beta)}} \quad (8)$$

Spectral thermometry, which includes two-color thermometry, multi-wavelength thermometry, and continuous spectrum thermometry, is analogous to two-color or multi-color image thermometry because the emissivity characteristics of the flame are needed. As an example, temperature can be calculated by the two-color method of spectral thermometry through the relationship between the radiation intensity at two adjacent wavelengths, as in Formula (9) [137]:

$$\frac{I(\lambda, T)}{I(\lambda + \Delta\lambda, T)} = \frac{\varepsilon(\lambda)}{\varepsilon(\lambda + \Delta\lambda)} \cdot \frac{(\lambda + \Delta\lambda)^5}{\lambda^5} \cdot \exp \left[ \frac{C_2}{T} \left( \frac{1}{\lambda + \Delta\lambda} - \frac{1}{\lambda} \right) \right] \quad (9)$$

where  $\Delta\lambda$  represents the interval between adjacent wavelengths in m. The emissivity at adjacent wavelengths is usually assumed to be about equal (i.e., grey-body hypothesis), so that Formula (9) can be further simplified with only unknown *T*, which can be directly calculated as:

$$T = C_2 \left( \frac{1}{\lambda + \Delta\lambda} - \frac{1}{\lambda} \right) / \ln \left[ \frac{I(\lambda, T)}{I(\lambda + \Delta\lambda, T)} \cdot \frac{\lambda^5}{(\lambda + \Delta\lambda)^5} \right] \quad (10)$$

Based on the above-mentioned basic theory of spectral temperature

measurement, some researchers have applied it to the measurement of flame temperature in the actual fuel combustion process [138–140]. The research group of Zhou [141–144] has carried out a series of systematic studies on the detection and reconstruction of temperature and soot volume measurement based on radiation emissions for different types of flame. Furthermore, they applied the method to a pulverized-coal-fired boiler furnace of a 200 MW power generation unit. Further, a 3-D temperature distribution of combustion was visualized (Fig. 12). A simultaneously reconstructed, three-dimensional temperature and radiative properties distribution in a pilot tubular furnace [145] and a 600 MW supercritical arch-fired boiler [146] were reported. The results show that online temperature detection based on flame image processing technology performs satisfactorily, and it is used for industrial combustion diagnostics.

Radiative emission is a great non-contact technique for temperature measurement. Not only is it used in high-temperature and other harsh environments, but it also offers advantages in constructing a multi-dimensional temperature field and reflecting combustion process characteristics. These are of great significance for the diagnostics of boiler furnaces and internal combustion engines. On the other hand, these methods generally rely on emissivity models, and their accuracy and reliability under different radiation conditions need to be investigated. Also, the existence of fly ash and other particles in the actual detection environment has a major impact on the target temperature measurement. Given the application value in the field of combustion process diagnostics, the development of a relatively simple and low-cost way to reconstruct a multi-dimensional temperature field is worthy of more investigation.

### 3.1.3. Measurements of free radicals and alkali metals

The emission spectrum produced from free radicals is able to reveal the combustion chemical reaction, and therefore, is another major indicator of the combustion process. Free radicals are unstable structures that readily react with other free radicals or molecules to form stable chemical bonds. Overall, they are short-lived and are challenging to detect. Some free radicals (e.g., OH, CH, and C<sub>2</sub>) emit relatively strongly in the UV–Vis range and are used to characterize flame intensity and structural distribution [147] and even to predict ignition time and to distinguish the type of fuels [148]. For example, CN and OH are usually used to characterize the generation of NO<sub>x</sub> [149], and the intensity ratios of HCO/C<sub>2</sub> and OH/C<sub>2</sub> can establish a certain relationship with CO emissions [150].

Alkali metals are widely present in a variety of fuels (e.g., coal and biomass). During the combustion process, the alkali metals are released

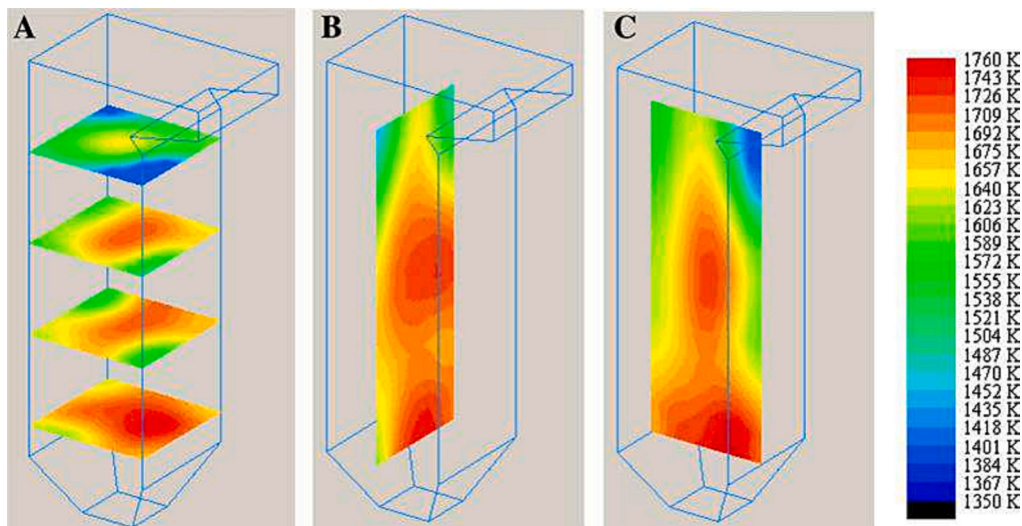


Fig. 12. Example of the 3-D temperature distribution inside a furnace [144].

in various forms, directly causing equipment issues such as scaling, slagging, and high-temperature corrosion of burners [151]. Therefore, it is of great significance to detect the release of alkali metals during the combustion process. It is well known that, owing to their low excitation potentials, alkali metals are easily excited in a flame. Details about the measurement of free radical and alkali metals in different flames through the radiative emission are summarized in Table 4.

In our previous work based on flame emission radiation, a series of investigations were conducted to reveal the release pattern of alkali metals during combustion. Different types of coal were prepared into a single coal pellet for experiments in different ambient conditions [163]. Ignition with a CO<sub>2</sub> laser was applied in this measurement. The emission spectrum of alkali metals was collected directly through a narrow slit of the spectrometer coupled with an ICCD. The temporal and spatial release behaviors of the alkalis were acquired. The results indicated that the release of the alkali metals is related to factors like the degree of coal carbonization, combustion atmosphere, and temperature. Also, in order to unveil the release behaviors of Na and K during the coal combustion process, an experiment was carried out with the use of single coal particles with variable additional amounts of K in different chemical forms (K<sub>2</sub>CO<sub>3</sub> and KCl) and in O<sub>2</sub>/N<sub>2</sub> and O<sub>2</sub>/CO<sub>2</sub> atmospheres [164]. The temporal release characteristics were obtained by the detection of Na and K emission spectra, and the main influence factors (flame temperature and elemental speciation) have been analyzed.

Overall, emission spectroscopy is effective for detection of free radicals in flames. The radiation intensities are strong enough for combustion diagnostics. We can infer the important reaction characteristics after proper processing of the emission signal. The types of free radicals that are present are greatly affected by the environment and the temperature. Furthermore, emission from some radical species is weak and could be difficult to detect. For alkali metals, their emission lines are overall intense; the key issue is how to overcome the impact of a complex combustion environment or to develop better spectral correction methods to improve prediction accuracy, and to establish a reliable relationship between the alkali-metal atomic emission and its concentration for real-world engineering applications.

### 3.2. LIBS for combustion diagnostics

#### 3.2.1. General

Laser diagnostics are used to obtain the intensity/concentration of the key species formed during combustion to gain more insight into the combustion process and mechanism. Sentko et al. [165] measured in-situ temperatures and H<sub>2</sub>O concentrations in laminar, premixed, fuel-rich, and quasi-adiabatic CH<sub>4</sub>/O<sub>2</sub>-flames by using tunable diode laser absorption spectroscopy (TDLAS) to understand the detailed chemistry mechanisms. Zhang et al. [166] developed a spectral-resolved laser-induced fluorescence (LIF) technique and analytic model to acquire polycyclic aromatic hydrocarbon (PAH) mole fractions in ethylene laminar premixed flames with different temperature profiles. Vestin et al. [167] presented the application of the polarization rotational coherent anti-Stokes Raman spectroscopy (CARS) approach to measure the temperature in the fuel-rich region of a diffusion flame and a premixed ethylene/oxygen/argon flame. Nevertheless, these approaches are used to obtain both the temperature and the specific composition information based on the specific wavelength of the incident laser. By contrast, in typical cases, many laser wavelengths can be used for LIBS and the wavelength does not need to be very specific, yet LIBS can provide multiple pieces of information effective for the diagnostics of combustion processes.

#### 3.2.2. Gas and liquid fuel combustion diagnostics

The basic gas fuel combustion is a homogeneous reaction process, including a premixed combustion flame and a diffused one. According to their flow characteristics, combustion flames can be described as laminar or turbulent. A premixed flame refers to one whose fuel and

**Table 4**  
Research details about the measurement of free radical and alkali metals.

Detecting object	Radical/atom	Research details	Ref.
CH <sub>4</sub> /O <sub>2</sub> co-flow jet diffusion flame	OH, CH, C <sub>2</sub>	The distribution of emission intensity of OH, CH, and C <sub>2</sub> of the co-jet diffusion flame was obtained, providing a theoretical basis for determining the reaction zone and quantifying the local O/C ratio of the flame.	[152]
Propane premixed flame	OH, CN, CH, C <sub>2</sub>	A system to simultaneously record OH, CN, CH, and C <sub>2</sub> radiation image of the flame. Air-fuel ratio was estimated by establishing the relationship with free radical emission intensity. The chemiluminescence signals of OH, HCO, CO <sub>2</sub> and the soot thermal radiation of the flame were identified. The correlation between OH intensity and exhaust NOx emission was explained, providing an effective method for the diagnostics of liquid fuel spray combustion and the formation of pollutants.	[153]
Butanol diesel blend flame	OH, HCO, CO <sub>2</sub>	The different combinations of emission intensity ratios between radicals were evaluated, and then correlation analysis was conducted with the emission of CO and NOx in the tail gas. Both HCO/C <sub>2</sub> and OH/C <sub>2</sub> ratios showed significant linear correlation with CO emission in certain conditions.	[154]
Diesel oil flame	OH, CH, C <sub>2</sub> , HCO, CH <sub>2</sub> O	Based on the analysis of the emission spectra and visual images of OH, NO, CN, and C <sub>2</sub> , as well as the 2-D temperature distribution of the flame, the high-temperature region and flame spread characteristics were specified, and the impact of key intermediate radicals on the formation of combustion products was revealed.	[150]
Pulverized coal flame/Jatropha oil flame	NO, OH, CN, C <sub>2</sub>	The emission intensity of alkali metal atoms released from biodiesel/ethanol flame was linearly correlated with the content of alkali metals in the fuel, and was not affected by the sample matrix.	[149,155]
Biodiesel flame	Na, K	The emission spectra and 2-D visual images of Na and K of the flame were obtained, showing that the flame emission spectrum was linked to the impinging region, atom type, alkali atom concentration, and flame temperature.	[156]
Diesel impinging flame	Na, K	The correlation between the release amounts in different stages and the peak release rates; the residual proportion of K in ash and the initial potassium content were extracted, providing support for the development of the K release model in the combustion process of biomass fuels.	[157]
Single particle flames of various biomass	K	The relative excited-state number densities for Na and K were derived from radiation data of alkali metals released from the	[158-159]
Sawdust flame	Na, K		[160]

(continued on next page)

Table 4 (continued)

Detecting object	Radical/atom	Research details	Ref.
Single particle flames of various biomass	CH, C <sub>2</sub> , Na, K	flame for quantitative analysis of alkali metals. The temporal evolution characteristic of CH, C <sub>2</sub> , Na, K chemiluminescence and the thermal radiation of soot and char were analyzed, which is helpful to clarify the ignition delay time and volatile combustion time and reveal the release pattern of alkali metals. OH signal was used to characterize flame height, reaction region, and pulsation intensity; OH/C <sub>2</sub> ratio was used to estimate the O/C. The feasibility of the two-color method in measuring the impact area flame temperature was verified.	[161–162]
Opposing impinging diesel flame	OH, CH, C <sub>2</sub> , Na, K, Ar	The emission spectra of H, CN, Na, K and Li can be seen as a sign of ignition. The 2-D distribution and emission intensity of OH were used to provide information on the reaction region and characterize the flame heat flow, respectively. The relationships between OH/CH, OH/C <sub>2</sub> ratio, O/C ratio, and mass flow rate of coal-water slurry were fitted, respectively, to provide support for combustion diagnostics.	[147]
Coal-water slurry diffusion flame	OH, CH, C <sub>2</sub> , CN, H, Na, K, Li		[148]

oxidizer are homogeneously mixed prior to ignition. The equivalence ratio of the flame is a critical parameter that relates to the combustion characteristics and the generation of pollutant species, such as CO and NO<sub>x</sub>. Multiple researchers have focused on the use of characteristic spectral-line ratios of H/O and C/(N + O), for example, to achieve

equivalence ratio measurements for laminar [168,169] or turbulent [170–172] combustion flames.

Because a laser beam can be tightly focused, LIBS provides satisfactory spatial resolution for flame diagnostics. Kiefer et al. [173] used LIBS to obtain spatially resolved equivalence ratios through H/N and H/O ratios in laminar premixed and non-premixed methane–air and dimethyl ether–air mixture flames. Lee et al. [174] analyzed two-dimensional LIBS profiles of liquefied petroleum gas (LPG) and electrolytic oxyhydrogen (EOH) flames to acquire chemical species information. The CN signal was used to identify the fuel concentration, and the H/O signal ratio was obtained to derive the fuel/air equivalent ratio. The above-mentioned spatial resolved diagnostic is based on the laser interaction for multiple flame positions. Wu et al. [175] used the horizontal and vertical dimensions of an ICCD array to provide spectral and spatial information, respectively. The temporal evolution of LIBS spectral-line images in a methane–air flame with an equivalence ratio  $\phi = 1$  for different laser energies is shown in Fig. 13. In each individual subplot, the horizontal axis represents the wavelength from 560 nm to 680 nm, and the vertical axis provides the spatially resolved distribution of the line emissions (~4 mm). It was found that for higher laser energy, the LIBS signal persists longer as a result of a denser plasma. This method was also successfully employed for 1-D fuel/air ratio measurements in both laminar and turbulent flames after calibration of the spatial distribution of the measured H/N ratio.

Laser-induced plasma provides multiple pieces of information (e.g., plasma temperature, emissions, and absorbed and transmitted energy), characterizing the properties of a substance. Lee and Hedge [176] were among the pioneers conducting flame thermometry with LIBS. Thereafter, Kiefer et al. [173,174,177] proposed the use of a breakdown threshold of laser pulse energy for flame thermometry and found that the acoustic and emission measurements are more sensitive to changes in flame temperature as a result of expansion characteristics and detector sensitivity [178]. Recently, Wu et al. [179] reported that the accompanying plasma-generated acoustic emission from laser-induced plasma shows a negative correlation with the flame temperature. Acoustic measurements were further conducted to evaluate the temperature distribution in an ethylene–air counter-flow flame with a large variation of temperature and composition. It was found that the differences between the measurement results and the numerical results are small. In our previous work [180], we employed an energy probe to measure plasma energy, which is defined as the reduction between the laser pulse energy and the transmitted energy. It can qualitatively

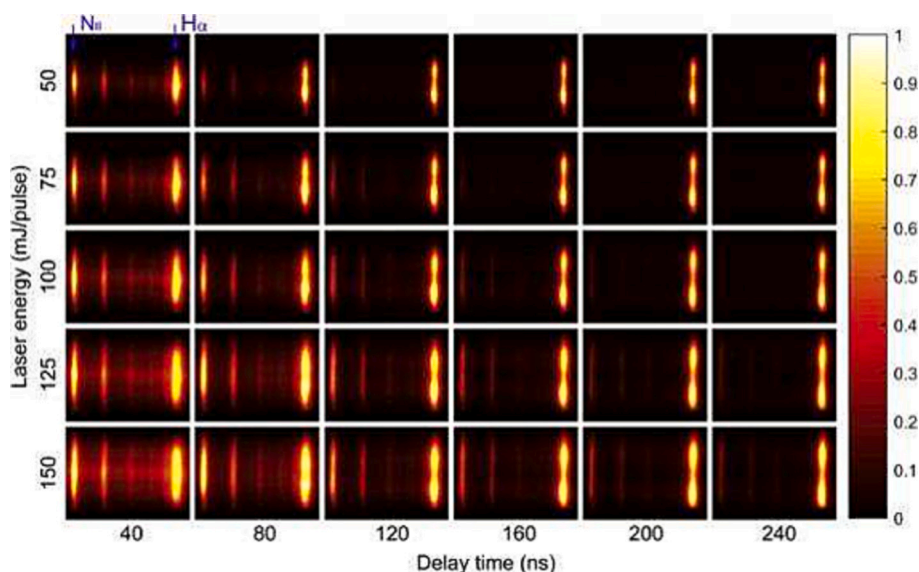


Fig. 13. Line-LIBS spectral images obtained in methane–air laminar flames with an equivalence ratio  $\phi = 1$  under different laser energies [175].

characterize the tendency of the temperature in the methane premixed flame. Subsequently, the different pieces of information (spectrum intensity, plasma energy, and equivalence ratio) were combined to reveal the distribution of a different flame region and the location of the flame front.

For liquid fuel combustion, LIBS is mainly focused on the measurement of fuel concentration and local equivalent ratio. Kim et al. [181] developed a portable device composed of photodiodes and bandpass filters to measure local fuel concentration in a liquid hydrocarbon-fueled spray flame and used the intensity ratios of H/O to present the local equivalence ratio of a gasoline–air mixture. Moreover, Lee et al. [174] used a two-dimensional LIBS mapping technique to provide the flame density, fuel concentration, and fuel/air equivalence ratio in the combustion of liquefied petroleum gas (LPG), LPG–EOH (electrolytic oxyhydrogen) mixture, and LPG–air mixture.

With the development of ultrafast lasers, LIBS with femtosecond (fs) lasers was introduced. Traditional nanosecond LIBS is considerably affected by laser intensity and focusing conditions. It is difficult to form molecular spectral lines because of the low intensity of the light field in the focusing region. Also, due to the long pulse width of a nanosecond laser, the interaction between laser and induced plasma (i.e., plasma shielding effect) makes it difficult to improve its signal-to-noise ratio. The femtosecond laser offers narrow pulse width and high peak power, with the potential to reduce the instabilities of the signal; its timing jitter can be as low as in the attosecond level [182], and it has also been reported for the measurement of equivalence ratios of various flames [183,184].

Furthermore, femtosecond laser filament occurs when the self-focusing caused by the Kerr effect and the defocusing caused by plasma ionization reach a dynamic equilibrium. Laser-induced filaments is a unique phenomenon that appears during the propagation of a high-intensity, ultrashort laser in a transparent medium [182], which has the possibility of multi-dimensional measurement. Zang et al. [185] studied the effects of laser energy and laser pulse repetition frequency on filament-induced spectra and found that one-dimensional equivalence ratio measurement is achievable under the condition of loose focusing. Li et al. [186,187] performed fs-LIPS in a methane/air co-flow piloted jet and found that the length of the plasma channel is about 15 mm and the spatial distribution is uniform. Two ICCD cameras were used to image the CH emission and the O I emission of the plasma channel, respectively; a good linear relationship was found between CH (431 nm)/O (777 nm) and the equivalence ratio, which indicates that fs-LIBS has an advantage in one-dimensional (line) measurements.

A remarkable number of studies have confirmed the feasibility of a rapid in-situ measurement of equivalence ratio by fs-LIBS. However, potential applications in the heat conversion process still need further exploration. For example, there is a need for quantitative detection of reaction intermediates or internal interaction mechanism with the femtosecond laser. Li et al. [188] found that the filament-induced fluorescence in the combustion flame mainly results from the interaction of femtosecond laser pulses with the combustion intermediates such as OH, CH, and C<sub>2</sub> but not from the direct fragmentation of the parent ethanol molecules. Therefore, it is necessary to further characterize the detailed interaction between the laser and the probed species for combustion diagnostics with LIBS.

### 3.2.3. Solid fuel combustion diagnostics

Recently, the application of LIBS in solid fuel combustion diagnostics was mainly for the measurement of alkali metals. To in-situ monitor the concentration of alkali elements (Na and K) in the plume of burning solid fuel particles using LIBS, a proper calibration is needed. Hsu et al. [189,190] and Yu et al. [191] proposed the use of a laminar premixed burner (Perkin Elmer) for the calibration of coal combustion. A nebulizer was used to produce fine aerosols of potassium sulfate (K<sub>2</sub>SO<sub>4</sub>) and sodium sulphite (Na<sub>2</sub>SO<sub>3</sub>) with a nominal diameter of 1 μm. In this setting, due to the specific arrangement of the present LIBS

measurement, as shown in Fig. 14, LIBS plasma was located inside the seeded flame and emission was collected through a lens and directed to a spectrometer. The self-absorption correction from the measured signals of the atomic species in the seed region around the LIBS plasma was based on the modified Beer-Lambert law. Subsequently, linear calibration curves were constructed for reliable measurements of [Na] total and [K] total in the flame environment. Based on the above calibration method, multiple works have been conducted to realize the quantitative analysis of Na and K released from burning coal particles in oxy-fuel combustion environments [192]. For example, the approach has been used to study the release characteristics of different classes of Na [193] and the release characteristics of alkali species during co-firing of coal and biomass [196]. The inhibition effects of addition minerals [194] and the effect of microwave radiation on the release of alkali metals [195] can also be revealed. Based on the online LIBS measurement information, the reaction pathway of alkali metals [197–200] can be acquired.

The aforementioned single-point LIBS method could provide the volatile sodium concentration at only one location per measurement. To overcome this limitation, Liu et al. [201–203] developed a multi-point LIBS method by fixing the focusing system of the laser lens and the acquisition system of the spectrometer on the same platform, as shown in Fig. 15. The high-precision stepper motor is mobile control; the dynamic LIBS measurement is realized without losing the measurement signal strength while keeping the movement direction of the platform consistent with the laser direction. They applied this method for quantitative measurement of Na concentrations in the plume during the burning of Zhundong coal particles and also proposed the combination of other techniques (Planar LIF and two-color pyrometry) with LIBS to measure the release of K during the combustion of biomass fuels (corn straw and poplar). An empirical model for the kinetics of potassium release was deduced to develop a map of potassium transformation processes during combustion [204].

In addition to alkali metals, we applied LIBS to study the combustion characteristics of the single coal particle by using CO<sub>2</sub> laser ignition, as shown in Fig. 16 [205]. The spatial distribution of H I, O I, and CN emission was obtained, and the residual energy was further measured to characterize the temperature profiles of combustion flames. It was found that the combustion stage discrimination (devolatilization, secondary reaction, and char combustion) is evidenced by the emission of H and CN. The correlation between the generation of CN and the NO<sub>x</sub> formation was presented to reveal the fuel-N conversion paths to better understand the combustion mechanism.

The above studies were based on pellet samples prepared as spherical shapes. To study the actual combustion process of the particles that might not be spherical, Li et al. [206,207] applied LIBS to characterize pulverized coal particle combustion with a Hencken burner. They proposed a new low-intensity, phase-selective LIBS (PS-LIBS) to distinguish the existence of Na in the particle or in the gas phase. Their low-intensity LIBS method is based on different breakdown thresholds between the gas phase and the particle phase and selectively shows only atoms in the particle phase, with no breakdown emission occurring for the gas phase. Moreover, Zhang et al. [208,209] also employed this method to analyze in-situ the formation of TiO<sub>2</sub> nanoparticles by vortex flame synthesis, including the measurement of the nanoparticle volume fraction for TiO<sub>2</sub> nanoparticles. To realize the 2-D image measurements, a cylindrical plano-convex lens of a focal length of 400 mm focused a laser sheet through a Bunsen burner. A bandpass filter was equipped to remove all other emission except for the Ti atomic emission around 500 nm, which is subsequently imaged by an ICCD [208]. The two-dimensional phase-selective LIBS imaging shows an adequate resolution of nanoparticle volume fraction variation in the boundary layer, influenced by diffusion and thermophoresis [208,210].

Overall, LIBS has made remarkable progress in the diagnostics of gas, liquid, and solid combustion flames. This technology is mainly used for flame equivalence ratio measurement, temperature detection, and alkali metal content and is a good match with LIBS in-situ and online

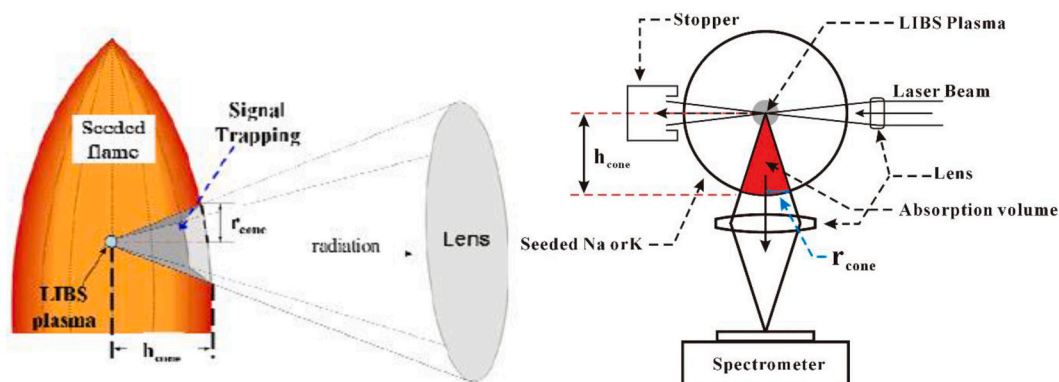


Fig. 14. Specific arrangement of the present LIBS measurement for flame measurement [189,190].

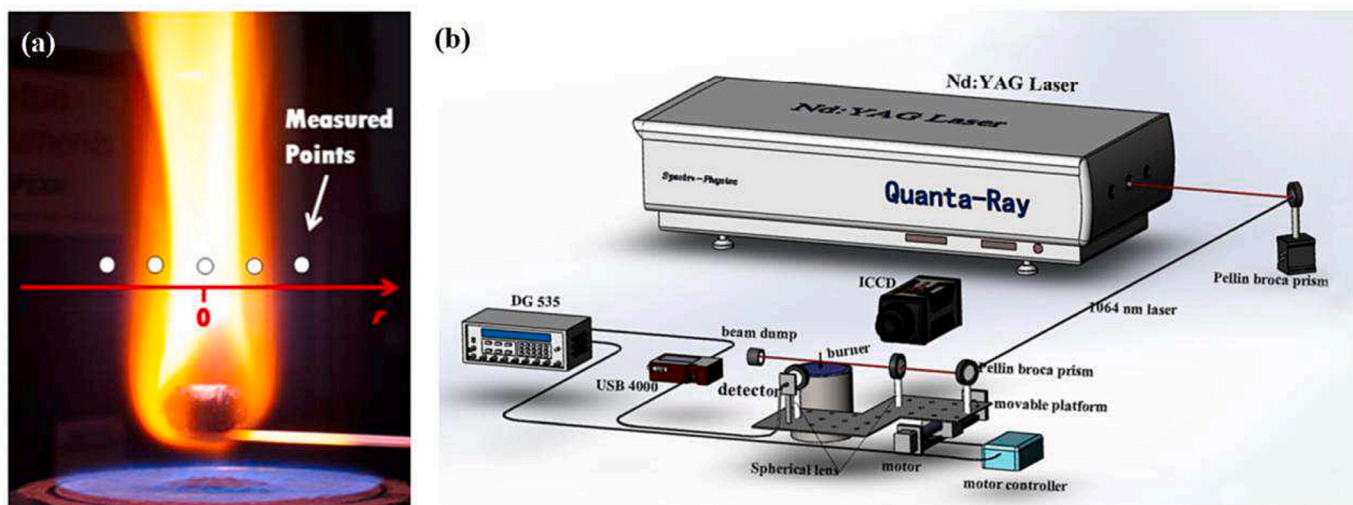


Fig. 15. Multi-point LIBS experiment setup: (a) LIBS measuring points and (b) configuration of equipment [201].

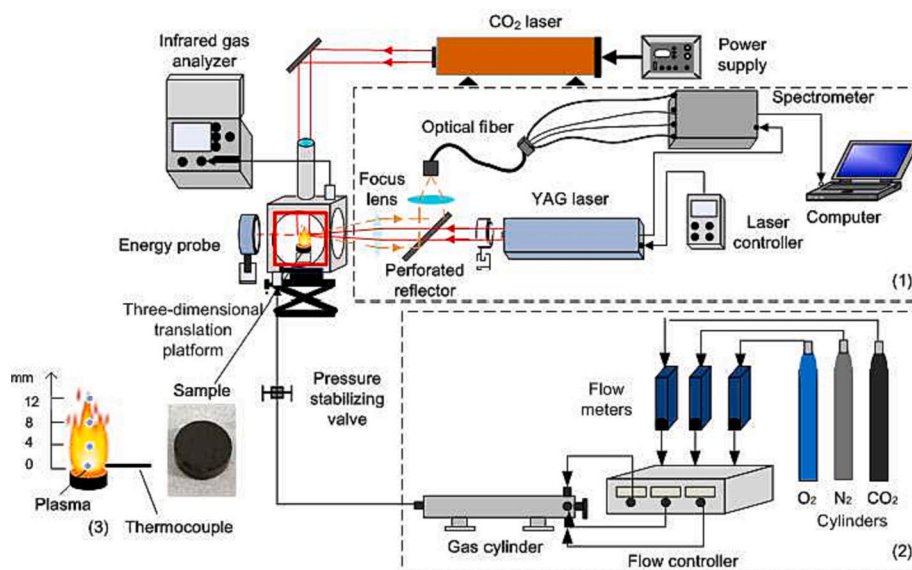


Fig. 16. LIBS system for single coal pellet by using CO<sub>2</sub> laser ignition: (1) LIBS setup, (2) gas system, and (3) positions of plasmas and thermocouple [205].

capabilities. However, there are still some technical obstacles to overcome. The commonly used ns-LIBS with low power density and long pulse duration would cause a low intensity of light field in the focus area and then lead to low repeatability and poor signal-to-noise ratio. In this context, a high-intensity femtosecond laser pulse is well able to overcome technical defects faced by traditional ns-LIBS, and fs-LIBS has a higher signal-to-noise ratio to detect the molecular groups.

Furthermore, the phase selective LIBS technology, which is based on the fact that the laser breakdown threshold of a particle phase is significantly lower than that of the gas phase, is used to measure particles in the flame through adjustment of the laser intensity to excite only the particle phase. The development of such advanced induced breakdown spectroscopy technologies lays the foundation for combustion diagnostics and deepens the understanding of combustion.

#### 4. LIBS for the combustion products

##### 4.1. General

Fly ash is the major component of the coal combustion products particularly in pulverized fuel combustion devices [211]. It is fine grained, and the powdery particulate material is generally recovered by electrostatic precipitation or mechanical filtration. The main composition of fly ash is Si, Al, Fe, Ca, and unburned carbon. Unburned carbon is an indicator of the combustion efficiency and a reference for optimizing boiler operation. The content of carbon and other elements in fly ash has to be measured and controlled for industrial production [212,213]. There are various methods for fly ash detection, including the thermal gravimetric analysis method, the microwave attenuation method, the electrostatic capacitance measurement method, and the loss-on-ignition (LOI) test. Moreover, X-ray diffraction (XRD) powder analysis or the scanning electron microscopy (SEM) method are also employed to deal with compositions and microstructure detection of the fly ash [214]. However, these methods cannot meet the needs of combustion optimization. The non-contact, fast-response LIBS technology was tested for the detection of components in fly ash, especially for the unburned carbon.

##### 4.2. Fundamental issue of LIBS for fly ash

Fly ash is a fragile fine-grained combustion byproduct that is difficult to be compacted into a pellet. Instead, the sample can be placed simply in a container or on a plane-like stainless steel disc. This no-sample-pretreatment approach simplifies the analysis procedure but brings with it uncertainties as to the laser-material interaction and the plasma evolution. The addition of binders is also a suitable approach to improve the mechanical strength of a sample for LIBS analysis. Ctvrtnickova et al. [215] carried out an investigation on the effect of different binders including potassium bromide (KBr), wax, and poly-vinyl alcohol (PVA) and sample deposition on the carbon tape. The use of tape was reported to be one of the fastest ways for sample preparation. Furthermore, the carbon-line intensity resulting from the ablation of the tape is negligible compared to the emission from the ash sample. Calibration curves were constructed for the emission from the majority of the elements (Ba, Mg, Ti, Fe, Si, and C) in the fly ash, and the KBr binder was found to be suitable for carbon calibration. Stankova et al. [216] used mixed binders (silver and cellulose, 1:1) to simultaneously improve the mechanical stability (cellulose) and element sensitivity (silver). A multi-matrix calibration curve was established with the use of reference materials. Good analytical results were reported with the use of an internal standard (carbon or silver). In conclusion, most of the current laboratory studies were based on the use of binders for sample preparation.

Our research group has also carried out a series of works on the application of LIBS for unburned carbon detection in fly ash [217–219]. The emission of C I 193.03 nm is weak; although the C I 247.86 nm line presents a stronger emission, it suffers spectral interference from a

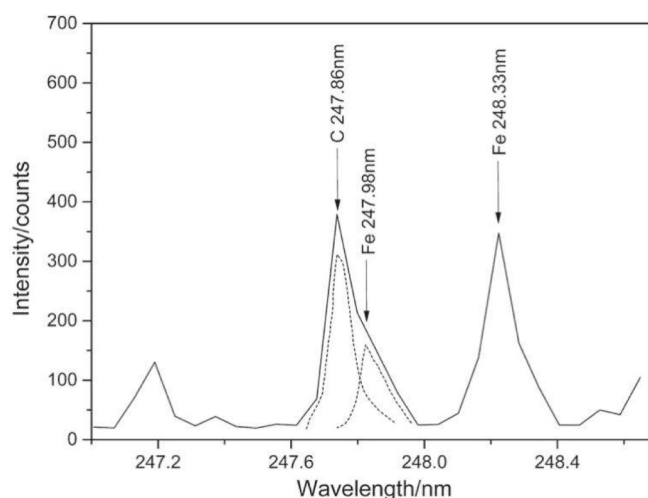


Fig. 17. Emission spectrum of C-Fe line interference [219].

nearby Fe line at 247.98 nm (Fig. 17 shows the overlapping peaks). To use the C I 247.86 nm line as a reference standard for quantitative analysis, a correction method using the Fe line to correct the C-Fe line interference was proposed. The basic criterion was that different spectral line intensities of the same element are related to plasma temperature. The intensity of the spectral-interfering Fe 247.98 nm line is first estimated from the non-interference Fe 248.33 nm line and then subtracted from the sum of the overlapping C–Fe lines to obtain the net C 247.86 nm emission [219].

Furthermore, molecular emission is another acceptable choice for carbon analysis. CN emission is mainly derived from the reaction between carbon-related species generated by sample ablation and nitrogen in air. Compared with the atomic C emission line, CN molecule emission is more stable and has fewer interference factors and therefore, can be used for the detection of unburned carbon content in fly ash. We proposed a method that utilizes CN emission as the analytical parameter and couples it with correction of plasma temperature and self-absorption. The averaged relative error of the prediction and the limit of detection achieved 0.26% and 0.16 wt%, respectively, which meets the measurement requirement of the PRC power industry standard [220].

##### 4.3. Actual industrial LIBS devices for fly ash

To apply LIBS for fly ash detection in actual production, Noda et al. [221] in 2002 developed an automated LIBS unit and conducted the application in actual power plant monitoring. Their work exhibited industrial capability for the analysis of carbon content in fly ash, char, and pulverized coal under high-pressure and high-temperature conditions. The plasma state variation in different operating conditions was corrected based on the ratio of ionic and atomic Mg lines. The measurement time was less than 1 min, which was acceptable for industrial application. Later, to achieve optimal and stable combustion, Kurihara et al. [222] established an automated LIBS unit that was composed of a sampling box and a control box as shown in Fig. 18. The researchers integrated it into a boiler-control system and applied it in a 1000-MW pulverized coal-fired power plant. Air dilution was used in the sampling module to reduce the interference of carbon dioxide from boiler exhaust with LIBS detection. Internal standardization with a Si line and plasma temperature correction compensates for the influence of plasma state and species concentration. The cyclone separator's (Cyclone 1 showed in Fig. 18) speed was adjusted in conjunction with the measured values of unburned carbon provided by the LIBS apparatus for boiler control optimization. The long-term operation of the equipment has proved its ability to analyze different types of coal fly ash.

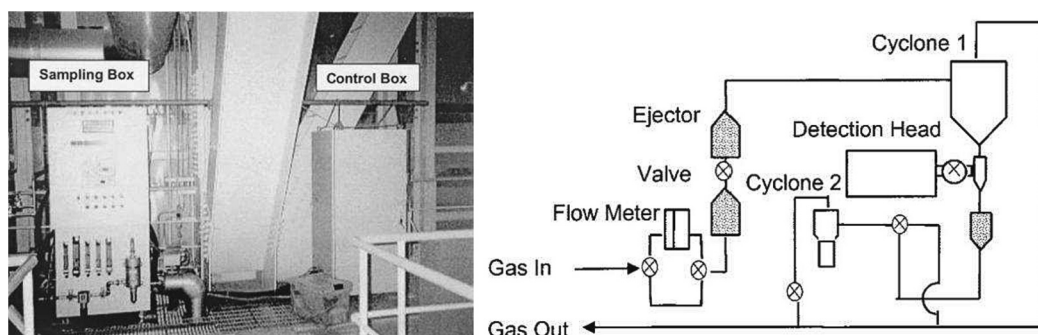


Fig. 18. Photograph of unburned-carbon measurement apparatus and the fly ash sampling system [222].

The presence of flue gas from actual combustion (e.g.,  $\text{CO}_2$ ) is not negligible and might interfere with the detection of the powder flow of fly ash. In this setting, Zhang et al. [223] developed a LIBS apparatus comprising an isokinetic sampler and a sample-preparation module, as shown in Fig. 19. This sampler performed interleaved sampling on two flues. Subsequently, the ash sample was conveyed to the measurement point using a conveying belt within the sample-preparation module. Setting gas inlet and outlet enabled the apparatus to remove the generated aerosols and  $\text{CO}_2$  from the measurement chamber by introducing an inert gas. Moreover, to improve the quantitative analysis results of unburned carbon, a second-order polynomial multivariate inverse regression was proposed to reduce the matrix effects. The achieved measurement accuracy was 0.26%, and the average relative error was 3.81%.

In actual equipment (e.g., boiler), fly ash generally exists in the form of particle flow. Wang et al. [124] applied LIBS for the direct measurement of fly ash particle flow. They measured the particle with different sizes separately to increase the detection accuracy. To further

enhance repeatability and precision, a correction factor for plasma signal was obtained and adopted depending on the optical setups, pressure, and buffer gas composition. The detection limit ( $S/N = 1$ ) of Fe, Al, and Ca in fly ash reached 0.1%, 0.3%, and 0.02%, respectively. Furthermore, the authors also focused on the effects of plasma states and coexisting materials (mainly for carbon dioxide) on quantitative measurement. The temperature of the plasma changed greatly as it evolved, so it was possible to establish corresponding temperature correction curves for the plasma signal in different temperature ranges to improve the analysis effectiveness [224,225]. A LIBS device containing a two-stage cyclone was developed as shown in Fig. 20a. The cyclone separator not only separated the exhausted steam and particles, but was also able to introduce the appropriate atmosphere according to the actual need. To evidence the  $\text{CO}_2$  effect on the unburned carbon measurement, the surrounding mixture gas of  $\text{N}_2$  and  $\text{CO}_2$  was directly introduced into the measurement chamber, as shown in Fig. 20b. Due to the different breakdown thresholds of gas and particle, a given laser energy and pulse width can effectively atomize and excite solid particles while avoiding air breakdown. The comparison of the measurement results with and without the presence of  $\text{CO}_2$  with lasers of pulse width of 6 ns and 1 ns showed that there was no evidence of a change in the spectra from fly ash with different  $\text{CO}_2$  concentrations using a laser with pulse width of 1 ns (Fig. 21b). However, the C signal intensity increased noticeably when 3.8%  $\text{CO}_2$  was introduced and measured with a laser of 6 ns pulse width (Fig. 21a). This indicates that the use of a laser with a shorter pulse width is an effective way to control the laser-induced particle plasma and the surrounding gas plasma [225].

In general, the development of LIBS apparatus showed the ability to perform reliable and real-time measurement of fly ash and provide a valuable support for boiler monitoring and optimization in coal-fired power plants. The development also significantly benefits the efficient treatment or utilization of fly ash. Future studies and application need to include an extensive discussion on the reliability and adaptability of the device and introduce changes according to the specific issues of proper adjustment in boiler operation. This will form a key part of industrial production, human health, and environmental protection.

## 5. Conclusion and outlook

For efficient and clean utilization of fuel, it is essential to obtain online measurements of the key parameters in the fuel heat utilization process and thereby master its dynamic characteristics. As a non-contact technology, optical measurement realizes in-situ continuous measurement of multiple parameters and significantly expands the possibility of detecting related components for combustion diagnostics in a real-time fashion. The present review focuses on the application of atomic emission spectroscopy, including LIBS and spontaneous emission spectroscopy, for the fuel thermal conversion process. In Section 2, LIBS as a potential online technology for characterization of raw energy material is discussed. Non-metallic elements play a significant role in defining the characteristics of energy materials. The section first analyzes the issues

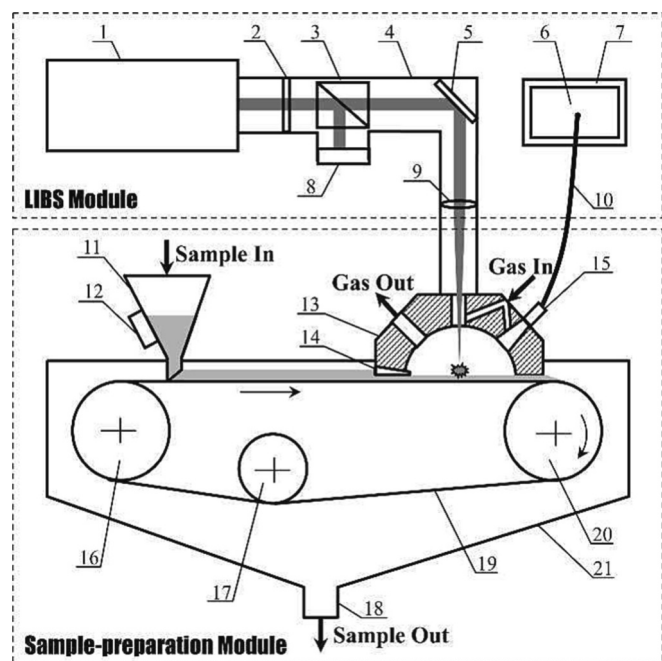


Fig. 19. LIBS device equipped with an isokinetic sampler and a sample-preparation module proposed by Zhang et al. [223]. The numbers are defined as follows: (1) Nd:YAG laser, (2) half-wave plate, (3) polarizing beam splitter, (4) bolt sleeve, (5) rear-silvered mirror, (6) spectrometer, (7) chiller, (8) energy meter, (9) focusing lens, (10) optical fiber, (11) conical funnel, (12) vibrator, (13) connection base, (14) smooth groove, (15) optical fiber splice, (16) driving pulley, (17) guide pulley, (18) cleanout door, (19) conveying belt, (20) drive pulley, and (21) shell.

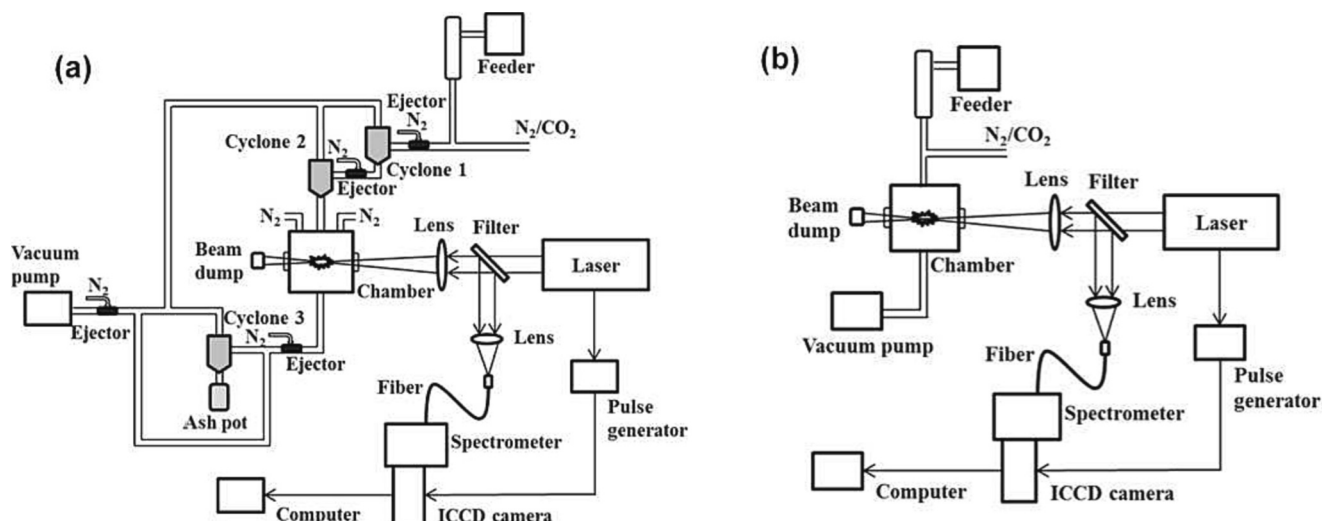


Fig. 20. Schematic diagram of the LIBS apparatus: (a) two-stage cyclone measurement system of fly ash flow and (b) direct measurement system of fly ash flow [225].

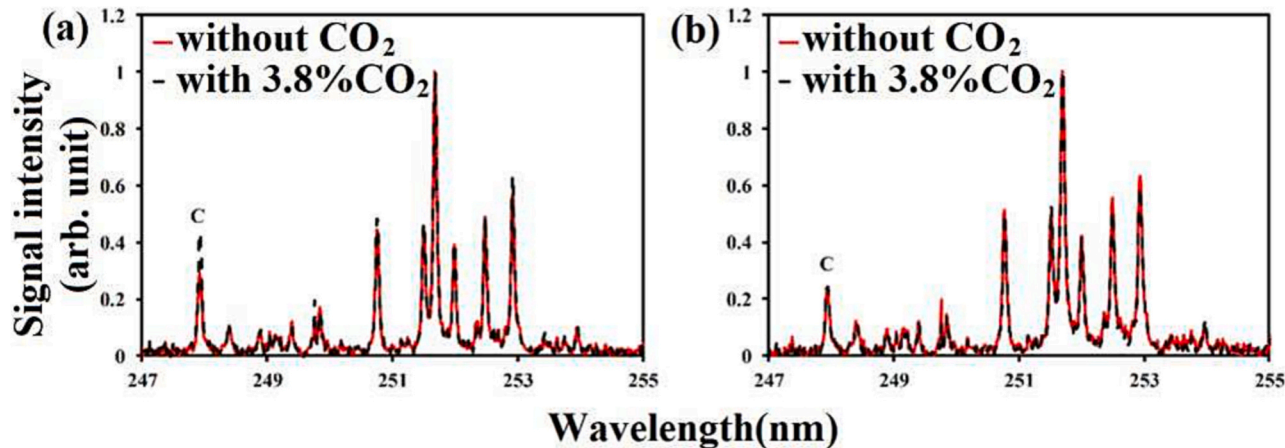


Fig. 21. Comparison of the measured spectra of fly ash with or without the  $\text{CO}_2$  condition: (a) spectra using a 6 ns pulse-width laser and (b) spectra using a 1 ns pulse-width laser [225].

of LIBS for nonmetal element detection. With coal as an example, it summarizes the characteristics of the process of main solid fuel detection. Next, the discussion focuses on the onsite application aspect with different sample forms (rock, pellet, particle flow). Although direct (i.e., no-sample-preparation) detection of particle flow for online measurements is desirable, there are two key issues. First, a stable sampling device, with continuous and stable particle flow during the measurement process, as well as its wear and blockage must be considered. Second, sample calibration issues need to be improved. At present, most powdered samples are transformed into pellets prior to an analysis, and the question of how to correct the spectrum from different sample forms needs to be addressed.

Section 3 presents the application of radiative emission and LIBS for combustion flame diagnostics. Radiative emission spectroscopy provides a simple and low-cost, non-contact way for measurement of temperature, free radicals, and alkali metals. However, the signal-to-noise is dependent on the radiation conditions, especially for the detection of free radicals. In the future, establishing different emissivity models and developing data processing algorithms and temperature correction methods, as well as applying artificial intelligence to identify complex detection environments, to eliminate strong interference and to identify the best calculation model will be beneficial to the development of

radiative temperature measurement. The introduction of LIBS to flame diagnostics improves the signal-to-noise ratio, but it is more difficult to achieve accurate quantitative measurement on the concentration of combustion-related species because of the matrix effect and the comparatively complex combustion environments. On this basis, femtosecond LIBS and phase selection LIBS have been developed, and they are of great significance for understanding the combustion process.

Section 4 focuses on the use of LIBS for the detection of combustion products – fly ash. The discussion includes the fundamental issue and actual industrial LIBS devices. The basic aspects are spectral interference, the direct formation of carbon-related molecular spectra, and the addition of binder. In terms of application, it mainly includes the development and field application of relevant online testing equipment. Overall, in order to realize online detection of the composition content of fly ash, attention should be paid to the following issues. First, the concentration of fly ash in the flue on-site is low, or the sampling of fly ash is more difficult. Second, the  $\text{CO}_2$  in the flue gas could interfere with the unburned carbon measurement.

Finally, the review concludes with a summary and discussion of further applications and directions for improvement. As outlined in this review, LIBS technology has been considered worldwide as a potential rapid/online detection technology for simultaneous multi-element

detection of sample components, but it is also still at the stage of mechanism research and technology development due to the uncertainty of point measurement and the development limitation of hardware equipment and system integration. To achieve real application, the environmental adaptability of the system and measurement accuracy need to be continuously optimized and improved. For combustion diagnostics, LIBS and spontaneous radiation can be used to obtain some information, but it is better to combine some other online techniques to acquire more information so as to understand the whole, complex combustion processes. All this work lays a foundation for subsequent research.

### Declaration of Competing Interest

There are no conflicts to declare.

### Data availability

No data was used for the research described in the article.

### Acknowledgments

The research was supported by the National Natural Science Foundation of China (No. 51976064) and the Guangdong Basic and Applied Basic Research Foundation (No. 2022A1515010709). We acknowledge the support from the Fundamental Research Funds for the Central Universities (2022ZFJH04) and the Guangdong Province Key Laboratory of Efficient and Clean Energy Utilization (2013A061401005).

### References

- [1] BP statistical review of world energy 2022, BP p.l.c, London, 2022.
- [2] W.M. Lewandowski, M. Rym, W. Kosakowski, Thermal biomass conversion: a review, *Processes*. 8 (2020) 516, <https://doi.org/10.3390/pr8050516>.
- [3] M. Haghghat, N. Majidian, A. Hallajisani, M. Samipourgiri, Production of bio-oil from sewage sludge: A review on the thermal and catalytic conversion by pyrolysis, *Sustain Energy Techn.* 42 (2020), 100870, <https://doi.org/10.1016/j.seta.2020.100870>.
- [4] M. Younis, S.Y. Alnouri, B.J. Abu Tarboush, M.N. Ahmad, Renewable biofuel production from biomass: a review for biomass pelletization, characterization, and thermal conversion techniques, *Int J Green, Energy*. 15 (2018) 837–863, <https://doi.org/10.1080/15435075.2018.1529581>.
- [5] A. Tchapda, S. Pisupati, A review of thermal co-conversion of coal and biomass/waste, *Energies*. 7 (2014) 1098–1148, <https://doi.org/10.3390/en7031098>.
- [6] <https://zh.wikibooks.org/zh-cn/File:PowerStation3.svg>.
- [7] Y. Zhang, X. Zhang, W. Jia, Q. Shan, Y. Li, D. Hei, D. Chen, Online x-ray fluorescence (XRF) analysis of heavy metals in pulverized coal on a conveyor belt, *Appl. Spectrosc.* 70 (2016) 272–278, <https://doi.org/10.1177/0003702815620129>.
- [8] M. Gräbner, E. Lester, Proximate and ultimate analysis correction for kaoliniferous Chinese coals using mineral liberation analysis, *Fuel*. 186 (2016) 190–198, <https://doi.org/10.1016/j.fuel.2016.08.074>.
- [9] M. Borsaru, M. Berry, M. Biggs, A. Rojc, In situ determination of sulphur in coal seams and overburden rock by PGNA, *Nucl. Instrum. Meth. B*. 213 (2004) 530–534, [https://doi.org/10.1016/S0168-583X\(03\)01623-9](https://doi.org/10.1016/S0168-583X(03)01623-9).
- [10] M. Borsaru, M. Biggs, W. Nichols, F.A.R. Bos, The application of prompt-gamma neutron activation analysis to borehole logging for coal, *Appl. Radiat. Isot.* 54 (2001) 335–343, [https://doi.org/10.1016/S0969-8043\(00\)00109-3](https://doi.org/10.1016/S0969-8043(00)00109-3).
- [11] L. Bartoňová, Unburned carbon from coal combustion ash: an overview, *Fuel Process. Technol.* 134 (2015) 136–158, <https://doi.org/10.1016/j.fuproc.2015.01.028>.
- [12] F. Peng, Y. Niu, K. Gao, X. Gai, L. Dai, L. Geng, Comparison of different microwave methods for unburned carbon content in fly ash determination, *Measurement*. 139 (2019) 346–354, <https://doi.org/10.1016/j.measurement.2019.02.061>.
- [13] H. Liu, H. Tan, Q. Gao, X. Wang, T. Xu, Microwave attenuation characteristics of unburned carbon in fly ash, *Fuel*. 89 (2010) 3352–3357, <https://doi.org/10.1016/j.fuel.2010.02.029>.
- [14] R. Noll, *Laser-Induced Breakdown Spectroscopy*, Springer, Berlin, Heidelberg, 2012.
- [15] D.A. Cremers, L.J. Radziemski, *Handbook of laser-induced breakdown spectroscopy*, John Wiley & Sons Ltd, Chichester, 2013, <https://doi.org/10.1002/9781118567371>.
- [16] D.A. Cremers, L.J. Radziemski, *Handbook of Laser-induced Breakdown Spectroscopy*, John Wiley & Sons Ltd, 2006, <https://doi.org/10.1002/0470093013>.
- [17] C. E. Romero, R. De Saro, LIBS Analysis for coal, In: S. Musazzi, U. Perini, (eds) *Laser-Induced Breakdown Spectroscopy*. Springer Series in Optical Sciences, vol 182. Springer, Berlin, Heidelberg. doi:[https://doi.org/10.1007/978-3-642-45085-3\\_19](https://doi.org/10.1007/978-3-642-45085-3_19).
- [18] B. Lemièrre, Y.A. Uvarova, New developments in field-portable geochemical techniques and on-site technologies and their place in mineral exploration, *Geochemistry: Exploration, Environment, Analysis*. 20 (2020) 205–216, <https://doi.org/10.1144/geochem2019-044>.
- [19] R. Harmon, C. Lawley, J. Watts, C. Harraden, A. Somers, R. Hark, Laser-induced breakdown spectroscopy—an emerging analytical tool for mineral exploration, *Minerals*. 9 (2019) 718, <https://doi.org/10.3390/min9120718>.
- [20] S.W. Hudson, J. Craparo, R. De Saro, D. Apelian, Applications of laser-induced breakdown spectroscopy (LIBS) in molten metal processing, *Metall. Mater. Trans. B Process Metall. Mater. Process. Sci.* 48 (2017) 2731–2742, <https://doi.org/10.1007/s11663-017-1032-7>.
- [21] L. Guo, D. Zhang, L. Sun, S. Yao, L. Zhang, Z. Wang, Q. Wang, H. Ding, Y. Lu, Z. Hou, Z. Wang, Development in the application of laser-induced breakdown spectroscopy in recent years: a review, *Front. Phys.* 16 (2021) 1–25, <https://doi.org/10.1007/s11467-020-1007-z>.
- [22] G.S. Senesi, R.S. Harmon, R.R. Hark, Field-portable and handheld laser-induced breakdown spectroscopy: Historical review, current status and future prospects, *Spectrochim. Acta B* 175 (2021), 106013, <https://doi.org/10.1016/j.sab.2020.106013>.
- [23] P.A. Gaviola, M. Sallèse, M. Suarez Anzorena, C.E. Ararat Ibarquén, A.A. Bertolo, M. Iribarren, R. Perez, E. Morel, J. Torga, A.J. Kreiner, M.F. del Grosso, Development of a simple method based on LIBS for evaluation of neutron production targets made of hydrogen isotopes, *Measurement*. 177 (2021), 109245, <https://doi.org/10.1016/j.measurement.2021.109245>.
- [24] M. Ghezelbash, A.E. Majd, S.M.R. Darbani, S.J. Mousavi, A. Ghasemi, M. K. Tehrani, Spatial investigation of plasma emission from laminar diffusion methanol, ethanol, and n-propanol alcohol flames using LIBS method, *Appl. Phys. B Lasers Opt.* 123 (2017) 1–14, <https://doi.org/10.1007/s00340-016-6615-5>.
- [25] F. Dong, X. Chen, Q. Wang, L. Sun, H. Yu, Y. Liang, J. Wang, Z. Ni, Z. Du, Y. Ma, J. Lu, Recent progress on the application of LIBS for metallurgical online analysis in China, *Front. Phys.* 7 (2012) 679–689, <https://doi.org/10.1007/s11467-012-0263-y>.
- [26] H. Pawlak-Kruczek, A. Arora, A. Gupta, M.A. Saeed, L. Niedzwiecki, G. Andrews, H. Phylaktou, B. Gibbs, A. Nowaczyk, P.M. Livesey, Biocoal - Quality control and assurance, *Biomass Bioenergy* 135 (2020), 105509, <https://doi.org/10.1016/j.biombioe.2020.105509>.
- [27] D.T. Chadwick, K.P. McDonnell, L.P. Brennan, C.C. Fagan, C.D. Everard, Evaluation of infrared techniques for the assessment of biomass and biofuel quality parameters and conversion technology processes: A review, *Renew. Sust. Energ. Rev.* 30 (2014) 672–681, <https://doi.org/10.1016/j.rser.2013.11.006>.
- [28] F.R. Amin, Y. Huang, Y. He, R. Zhang, G. Liu, C. Chen, Biochar applications and modern techniques for characterization, *Clean Technol. Environ. Res.* 18 (2016) 1457–1473, <https://doi.org/10.1007/s10098-016-1218-8>.
- [29] P.E. Sudol, K.M. Pierce, S.E. Prebihalo, K.J. Skogerboec, B.W. Wrightd, R. E. Synovec, Development of gas chromatographic pattern recognition and classification tools for compliance and forensic analyses of fuels: A review, *Anal. Chim. Acta* 1132 (2020) 157–186, <https://doi.org/10.1016/j.aca.2020.07.027>.
- [30] C. Liu, L. Xu, Laser absorption spectroscopy for combustion diagnostics in reactive flows: A review, *Appl. Spectrosc. Rev.* 54 (2018) 1–44, <https://doi.org/10.1080/05704928.2018.1448854>.
- [31] R.V. Ravikrishna, A.B. Sahu, Advances in understanding combustion phenomena using non-premixed and partially premixed counterflow flames: a review, *Int. J. Spray Combust.* 10 (2017) 38–71, <https://doi.org/10.1177/1756827717738168>.
- [32] F. Xing, Y. Huang, M. Zhao, J. Zhao, The brief introduction of different laser diagnostics methods used in aeroengine combustion research, *J. Sensors*. 42 (2016) 1660184, <https://doi.org/10.1142/S2010194516601848>.
- [33] K. Zhan, J. Chen, C. He, Z. Tang, Q. Li, K. Liu, C. Zhu, X. Li, Study on the spectral characteristics and analytical performance of pulverized coal using laser-induced breakdown spectroscopy under a fast physical constraint, *J. Anal. Atom. Spectrom.* 36 (2021) 1210–1216, <https://doi.org/10.1039/D1JA00047K>.
- [34] Y. Zhao, L. Zhang, S. Zhao, Y. Li, Y. Gong, L. Dong, W. Ma, W. Yin, S. Yao, J. Lu, L. Xiao, S. Jia, Review of methodological and experimental LIBS techniques for coal analysis and their application in power plants in China, *Front. Phys.* 11 (2016), 114211, <https://doi.org/10.1007/s11467-016-0600-7>.
- [35] Z. Wang, T. Yuan, Z. Hou, W. Zhou, J. Lu, H. Ding, X. Zeng, Laser-induced breakdown spectroscopy in China, *Front. Phys.* 9 (2013) 419–438, <https://doi.org/10.1007/s11467-013-0410-0>.
- [36] S. Sheta, M.S. Afgan, Z. Hou, S. Yao, L. Zhang, Z. Li, Z. Wang, Coal analysis by laser-induced breakdown spectroscopy: a tutorial review, *J. Anal. Atom. Spectrom.* 34 (2019) 1047–1082, <https://doi.org/10.1039/C9JA00016J>.
- [37] H. Peng, G. Chen, X. Chen, Z. Lu, S. Yao, Hybrid classification of coal and biomass by laser-induced breakdown spectroscopy combined with K-means and SVM, *Plasma Sci. Technol.* 21 (2018), 034008, <https://doi.org/10.1088/2058-6272/aaebc4>.
- [38] Z. Lu, X. Chen, S. Yao, H. Qin, L. Zhang, X. Yao, Z. Yu, J. Lu, Feasibility study of gross calorific value, carbon content, volatile matter content and ash content of solid biomass fuel using laser-induced breakdown spectroscopy, *Fuel*. 258 (2019), 116150, <https://doi.org/10.1016/j.fuel.2019.116150>.
- [39] J. Ibarra, E. Munoz, R. Moliner, FTIR study of the evolution of coal structure during the coalification process, *Org. Geochem.* 24 (1996) 725–735, [https://doi.org/10.1016/0146-6380\(96\)00063-0](https://doi.org/10.1016/0146-6380(96)00063-0).

- [40] NIST, Standard Reference Database 78. <https://www.nist.gov/pml/atom-ic-spectra-database>.
- [41] L. Zhang, L. Dong, H. Dou, W. Yin, S. Jia, Laser-induced breakdown spectroscopy for determination of the organic oxygen content in anthracite coal under atmospheric conditions, *Appl. Spectrosc.* 62 (2008) 458–463, <https://doi.org/10.1366/000370208784046786>.
- [42] M. Dong, J. Long, S. Chen, L. Wei, W. Li, W. Chen, S. Chen, J. Yu, J. Lu, Laser-induced molecular spectroscopy for carbon with different element speciation, *Acta Photon. Sinic.* 47 (2018), 847001, <https://doi.org/10.3788/gzxb20184708.0847001>.
- [43] J. Li, J. Lu, Z. Lin, S. Gong, C. Xie, L. Chang, L. Yang, P. Li, Effects of experimental parameters on elemental analysis of coal by laser-induced breakdown spectroscopy, *Opt. Laser Technol.* 41 (2009) 907–913, <https://doi.org/10.1016/j.optlastec.2009.03.003>.
- [44] Z. Wang, T. Yuan, S. Lui, Z. Hou, X. Li, Z. Li, W. Ni, Major elements analysis in bituminous coals under different ambient gases by laser-induced breakdown spectroscopy with PLS modeling, *Front. Phys.* 7 (2012) 708–713, <https://doi.org/10.1007/s11467-012-0262-z>.
- [45] J. Moros, J. Laserna, Laser-induced breakdown spectroscopy (LIBS) of organic compounds: a review, *Appl. Spectrosc.* 73 (2019) 963–1011, <https://doi.org/10.1364/AS.73.000963>.
- [46] M. Dong, J. Lu, S. Yao, Z. Zhong, J. Li, J. Li, W. Lu, Experimental study on the characteristics of molecular emission spectroscopy for the analysis of solid materials containing C and N, *Opt. Express* 19 (2011) 17021–17029, <https://doi.org/10.1364/OE.19.017021>.
- [47] L.M. Cabalin, T. Delgado, L. Garcia-Gomez, J.J. Laserna, Considerations on formation mechanisms of emitting species of organic and C-containing inorganic compounds in CO<sub>2</sub> atmosphere using laser-induced breakdown spectroscopy as a strategy for detection of molecular solids, *Spectrochim. Acta B* 169 (2020), 105869, <https://doi.org/10.1016/j.sab.2020.105869>.
- [48] C. Vivien, J. Hermann, A. Perrone, C. Boulmer-Leborgne, A study of molecule formation during laser ablation of graphite in low-pressure nitrogen, *J. Phys. D: Appl. Phys.* 31 (1998) 1263–1272, <https://doi.org/10.1088/0022-3727/31/10/019>.
- [49] W. Zhu, X. Li, R. Sun, Z. Cao, M. Yuan, L. Sun, X. Yu, J. Wu, Investigation of the CN and C<sub>2</sub> emission characteristics and microstructural evolution of coal to char using laser-induced breakdown spectroscopy and Raman spectroscopy, *Energy* 240 (2022), 122827, <https://doi.org/10.1016/j.energy.2021.122827>.
- [50] M. Dong, G.C.Y. Chan, X. Mao, J.J. Gonzalez, J. Lu, R.E. Russo, Elucidation of C<sub>2</sub> and CN formation mechanisms in laser-induced plasmas through correlation analysis of carbon isotopic ratio, *Spectrochim. Acta B* 100 (2014) 62–69, <https://doi.org/10.1016/j.sab.2014.08.009>.
- [51] M. Dong, L. Wei, J. Lu, W. Li, S. Lu, S. Li, C. Liu, J.H. Yoo, A comparative model combining carbon atomic and molecular emissions based on partial least squares and support vector regression correction for carbon analysis in coal using LIBS, *J. Anal. Atom. Spectrom.* 34 (2019) 480–488, <https://doi.org/10.1039/C8JA00414E>.
- [52] M. Dong, X. Mao, J.J. Gonzalez, J. Lu, R.E. Russo, Time-resolved LIBS of atomic and molecular carbon from coal in air, argon and helium, *J. Anal. Atom. Spectrom.* 27 (2012) 2066–2075, <https://doi.org/10.1039/C2JA30222E>.
- [53] H. Rajavelu, N.J. Vasa, S. Seshadri, Laser-induced breakdown spectroscopy combined with temporal plasma analysis of C<sub>2</sub> molecular emission for carbon analysis in coal, *Appl. Spectrosc.* 75 (7) (2021) 893–900, <https://doi.org/10.1177/00037028211012399>.
- [54] M. Chen, T. Yuan, Z. Hou, Z. Wang, Y. Wang, Effects of moisture content on coal analysis using laser-induced breakdown spectroscopy, *Spectrochim. Acta B* 112 (2015) 23–33, <https://doi.org/10.1016/j.sab.2015.08.003>.
- [55] S. Yao, J. Zhao, Z. Wang, Y. Deguchi, Z. Lu, J. Lu, Analysis of spectral properties for coal with different volatile contents by laser-induced breakdown spectroscopy, *Spectrochim. Acta B* 149 (2018) 249–255, <https://doi.org/10.1016/j.sab.2018.09.002>.
- [56] J. Cai, M. Dong, Y. Zhang, Y. Chen, Y. Liang, J. Lu, Temporally and spatially resolved study of laser-induced plasma generated on coals with different volatile matter contents, *Spectrochim. Acta B* 180 (2021), 106195, <https://doi.org/10.1016/j.sab.2021.106195>.
- [57] W. Zhang, Z. Zhuo, P. Lu, J. Tang, H. Tang, J. Lu, T. Xing, Y. Wang, LIBS analysis of the ash content, volatile matter, and calorific value in coal by partial least squares regression based on ash classification, *J. Anal. Atom. Spectrom.* 35 (2020) 1621–1631, <https://doi.org/10.1039/D0JA00186D>.
- [58] X. Li, Y. Yang, G. Li, B. Chen, W. Hu, Accuracy improvement of quantitative analysis of calorific value of coal by combining support vector machine and partial least square methods in laser-induced breakdown spectroscopy, *Plasma Sci. Technol.* 22 (2020), 074014, <https://doi.org/10.1088/2058-6272/ab8972>.
- [59] M. Gaft, E. Dvir, H. Modiano, U. Schone, Laser induced breakdown spectroscopy machine for online ash analyses in coal, *Spectrochim. Acta B* 63 (2008) 1177–1182, <https://doi.org/10.1088/2058-6272/ab8972>.
- [60] M. Gaft, I. Sapir-Sofer, H. Modiano, R. Stana, Laser induced breakdown spectroscopy for bulk minerals online analyses, *Spectrochim. Acta B* 62 (2007) 1496–1503, <https://doi.org/10.1016/j.sab.2007.10.041>.
- [61] C.E. Romero, R. De Saro, J. Craparo, A. Weisberg, R. Moreno, Z. Yao, Laser-induced breakdown spectroscopy for coal characterization and assessing slagging propensity, *Energy Fuel* 24 (2010) 510–517, <https://doi.org/10.1021/ef900873w>.
- [62] C.E. Romero, Z. Yao, R. De Saro, J. Craparo, S. Lam, R. Silfies, R. Plangeman, F. Lyter, K. Quinty, Development and demonstration of laser-induced breakdown spectroscopy for in-situ, on-line coal analysis, *Intern. Pittsburgh Coal Conf.* (2011) 12–15.
- [63] D. Redoglio, E. Golinelli, S. Musazzi, U. Perini, F. Barberis, A large depth of field LIBS measuring system for elemental analysis of moving samples of raw coal, *Spectrochim. Acta B* 116 (2016) 46–50, <https://doi.org/10.1016/j.sab.2015.11.005>.
- [64] D.A. Redoglio, E. Golinelli, S. Musazzi, U. Perini, F. Barberis, Development of a large depth of field collection optics for on-line Laser-Induced Breakdown Spectroscopy applications, *Spectrochim. Acta B* 123 (2016) 179–183, <https://doi.org/10.1016/j.sab.2016.07.009>.
- [65] L. Yu, J. Lu, W. Chen, G. Wu, K. Shen, W. Feng, Analysis of pulverized coal by laser-induced breakdown spectroscopy, *Plasma, Sci. Technol.* 7 (2005) 3041–3044, <https://doi.org/10.1088/1009-0630/7/5/015>.
- [66] S. Yao, J. Zhao, J. Xu, Z. Lu, J. Lu, Optimizing the binder percentage to reduce matrix effects for the LIBS analysis of carbon in coal, *J. Anal. Atom. Spectrom.* 32 (2017) 766–772, <https://doi.org/10.1039/C6JA00458J>.
- [67] T. Yuan, Z. Wang, L. Li, Z. Hou, Z. Li, W. Ni, Quantitative carbon measurement in anthracite using laser-induced breakdown spectroscopy with binder, *Appl. Opt.* 51 (2012) B22–B29, <https://doi.org/10.1364/AO.51.000B22>.
- [68] M.P. Mateo, G. Nicolas, A. Yañez, Characterization of inorganic species in coal by laser-induced breakdown spectroscopy using UV and IR radiations, *Appl. Surf. Sci.* 254 (2007) 868–872, <https://doi.org/10.1016/j.apsusc.2007.08.043>.
- [69] X. Wang, L. Zhang, J. Fan, Y. Li, Y. Gong, L. Dong, W. Ma, W. Yin, S. Jia, Parameters optimization of laser-induced breakdown spectroscopy experimental setup for the case with beam expander, *Plasma Sci. Technol.* 17 (2015) 914–918, <https://doi.org/10.1088/1009-0630/17/11/04>.
- [70] X. Li, Z. Wang, Y. Fu, Z. Li, W. Ni, Wavelength dependence in the analysis of carbon content in coal by nanosecond 266 nm and 1064 nm laser induced breakdown spectroscopy, *Plasma Sci. Technol.* 17 (2015) 621–624, <https://doi.org/10.1088/1009-0630/17/8/02>.
- [71] H. Qin, Z. Yu, Z. Lu, Z. Yu, S. Yao, Exploiting data uncertainty for improving the performance of a quantitative analysis model for laser-induced breakdown spectroscopy, *Appl. Spectrosc.* 6 (2022) 1–9, <https://doi.org/10.1177/00037028221108416>.
- [72] Y. Liu, D. Wang, X. Ren, Rapid quantitation of coal proximate analysis by using laser-induced breakdown spectroscopy, *Energies* 15 (2022) 2728, <https://doi.org/10.3390/en15082728>.
- [73] W. Zhu, X. Li, R. Sun, Y. Zhang, Y. Yan, X. Yu, X. Ren, Investigation of mineral-element migration upon pyrolysis and quantitative prediction of volatiles in coal using laser-induced breakdown spectroscopy, *J. Anal. Atom. Spectrom.* 36 (2021) 1399–1409, <https://doi.org/10.1039/D1JA00099C>.
- [74] W. Gu, W. Song, G. Yan, Q. Ye, Z. Li, M.S. Afgan, J. Liu, Y. Song, Z. Hou, Z. Wang, Z. Li, A data preprocessing method based on matrix matching for coal analysis by laser-induced breakdown spectroscopy, *Spectrochim. Acta B* 180 (2021), 106212, <https://doi.org/10.1016/j.sab.2021.106212>.
- [75] J. Chen, K. Zhan, Q. Li, Z. Tang, C. Zhu, K. Liu, X. Li, Spectral clustering based on histogram of oriented gradient (HOG) of coal using laser-induced breakdown spectroscopy, *J. Anal. Atom. Spectrom.* 36 (2021) 1297–1305, <https://doi.org/10.1039/D1JA00104C>.
- [76] W. Song, Z. Hou, M.S. Afgan, W. Gu, H. Wang, J. Cui, Z. Wang, Y. Wang, Validated ensemble variable selection of laser-induced breakdown spectroscopy data for coal property analysis, *J. Anal. Atom. Spectrom.* 36 (2021) 111–119, <https://doi.org/10.1039/D0JA00386G>.
- [77] P. Lu, Z. Zhuo, W. Zhang, J. Tang, Y. Wang, H. Zhou, X. Huang, T. Sun, J. Lu, A hybrid feature selection combining wavelet transform for quantitative analysis of heat value of coal using laser-induced breakdown spectroscopy, *Appl. Phys. B-Lasers O.* 127 (2021) 1–11, <https://doi.org/10.1007/s00340-020-07556-8>.
- [78] Y. Zhang, Z. Xiong, Y. Ma, C. Zhu, R. Zhou, X. Li, Q. Li, Q. Zeng, Quantitative analysis of coal quality by laser-induced breakdown spectroscopy assisted with different chemometric methods, *Anal. Methods* 12 (2020) 3530–3536, <https://doi.org/10.1039/D0AY00905A>.
- [79] Y. Zhang, M. Dong, L. Cheng, L. Wei, J. Cai, J. Lu, Improved measurement in quantitative analysis of coal properties using laser induced breakdown spectroscopy, *J. Anal. Atom. Spectrom.* 35 (2020) 810–818, <https://doi.org/10.1039/C9JA00429G>.
- [80] C. Yan, J. Qi, J. Liang, T. Zhang, H. Li, Determination of coal properties using laser-induced breakdown spectroscopy combined with kernel extreme learning machine and variable selection, *J. Anal. Atom. Spectrom.* 33 (2018) 2089–2097, <https://doi.org/10.1039/C8JA00284C>.
- [81] W. Li, J. Lu, M. Dong, S. Lu, J. Yu, S. Li, J. Huang, J. Liu, Quantitative analysis of calorific value of coal based on spectral preprocessing by laser-induced breakdown spectroscopy (LIBS), *Energy Fuel* 32 (2017) 24–32, <https://doi.org/10.1021/acs.energyfuels.7b01718>.
- [82] A. Li, S. Guo, N. Wazir, K. Chai, L. Liang, M. Zhang, Y. Hao, P. Nan, R. Liu, Accuracy enhancement of laser induced breakdown spectra using permittivity and size optimized plasma confinement rings, *Opt. Express* 25 (2017) 27559–27569, <https://doi.org/10.1364/OE.25.027559>.
- [83] J. Wei, J. Dong, T. Zhang, Z. Wang, H. Li, Quantitative analysis of the major components of coal ash using laser induced breakdown spectroscopy coupled with a wavelet neural network (WNN), *Anal. Methods* 8 (2016) 1674–1680, <https://doi.org/10.1039/C5AY02994E>.
- [84] Z. Hou, Z. Wang, T. Yuan, J. Liu, Z. Li, W. Ni, A hybrid quantification model and its application for coal analysis using laser induced breakdown spectroscopy, *J. Anal. Atom. Spectrom.* 31 (2016) 722–736, <https://doi.org/10.1039/C5JA00475F>.

- [85] L. Zhang, Y. Gong, Y. Li, X. Wang, J. Fan, L. Dong, W. Ma, W. Yin, S. Jia, Development of a coal quality analyzer for application to power plants based on laser-induced breakdown spectroscopy, *Spectrochim. Acta B* 113 (2015) 167–173, <https://doi.org/10.1016/j.sab.2015.09.021>.
- [86] T. Yuan, Z. Wang, S. Lui, Y. Fu, Z. Li, J. Liu, W. Ni, Coal property analysis using laser-induced breakdown spectroscopy, *J. Anal. Atom. Spectrom.* 28 (2013) 1045–1053, <https://doi.org/10.1039/C3JA50097G>.
- [87] A.F.M.Y. Haider, M.A. Rony, K.M. Abedin, Determination of the ash content of coal without ashing: a simple technique using laser-induced breakdown spectroscopy, *Energy Fuel* 27 (2013) 3725–3729, <https://doi.org/10.1021/ef400566u>.
- [88] M. Dong, J. Lu, S. Yao, J. Li, J. Li, Z. Zhong, W. Lu, Application of LIBS for direct determination of volatile matter content in coal, *J. Anal. Atom. Spectrom.* 26 (2011) 2183–2188, <https://doi.org/10.1039/C1JA10109A>.
- [89] S. Yao, J. Lu, M. Dong, K. Chen, J. Li, J. Li, Extracting coal ash content from laser-induced breakdown spectroscopy (LIBS) spectra by multivariate analysis, *Appl. Spectrosc.* 65 (2011) 1197–1201, <https://doi.org/10.1366/10-06190>.
- [90] S.M.Z. Iqbal, Z. Uddin, Z.A. Umar, N. Ahmed, R. Ahmed, M.A. Baig, Analysis of lakhra coal by calibration free laser-induced breakdown spectroscopy (CF-LIBS) and comparison of self-absorption correction procedures, *Anal. Lett.* (2021) 1–13, <https://doi.org/10.1080/00032719.2021.1910831>.
- [91] H. Rajavelu, N.J. Vasa, S. Seshadri, Effect of ambient on the coal characterization using laser-induced breakdown spectroscopy (LIBS), *Appl. Phys. A-Mater.* 126 (2020) 1–10, <https://doi.org/10.1007/s00339-020-03558-7>.
- [92] F. Deng, Y. Ding, Y. Chen, S. Zhu, F. Chen, Quantitative analysis of the content of nitrogen and sulfur in coal based on laser-induced breakdown spectroscopy: effects of variable selection, *Plasma Sci. Technol.* 22 (2020), <https://doi.org/10.1088/2058-6272/ab77d5>, 74005–074005.
- [93] Y. Ma, W. Zhang, Z. Xiong, H. Cui, Q. Li, R. Zhou, Y. Zhang, X. Li, X. Zeng, Q. Li, Accurate sulfur determination of coal using double-pulse laser-induced breakdown spectroscopy, *J. Anal. Atom. Spectrom.* 35 (2020) 1458–1463, <https://doi.org/10.1039/C9JA00448C>.
- [94] S.M.Z. Iqbal, Z. Uddin, N. Ahmed, Z.A. Umar, M.A. Baig, On the compositional analysis of Coal using calibration free laser induced breakdown spectroscopy, *Laser Phys.* 29 (2019), 036101, <https://doi.org/10.1088/1555-6611/aaff58>.
- [95] C. Yan, J. Qi, J. Ma, H. Tang, T. Zhang, H. Li, Determination of carbon and sulfur content in coal by laser induced breakdown spectroscopy combined with kernel-based extreme learning machine, *Chemometr. Intell. Lab.* 167 (2017) 226–231, <https://doi.org/10.1016/j.chemolab.2017.06.006>.
- [96] X. Li, H. Yin, Z. Wang, Y. Fu, Z. Li, W. Ni, Quantitative carbon analysis in coal by combining data processing and spatial confinement in laser-induced breakdown spectroscopy, *Spectrochim. Acta B* 111 (2015) 102–107, <https://doi.org/10.1016/j.sab.2015.07.007>.
- [97] X. Li, X. Mao, Z. Wang, R.E. Russo, Quantitative analysis of carbon content in bituminous coal by laser-induced breakdown spectroscopy using UV laser radiation, *Plasma, Sci. Technol.* 17 (2015) 928–932, <https://doi.org/10.1088/1009-0630/17/11/07>.
- [98] T. Yuan, Z. Wang, Z. Li, W. Ni, J. Liu, A partial least squares and wavelet-transform hybrid model to analyze carbon content in coal using laser-induced breakdown spectroscopy, *Anal. Chim. Acta* 807 (2014) 29–35, <https://doi.org/10.1016/j.aca.2013.11.027>.
- [99] X. Li, Z. Wang, Y. Fu, Z. Li, W. Ni, A model combining spectrum standardization and dominant factor based partial least square method for carbon analysis in coal using laser-induced breakdown spectroscopy, *Spectrochim. Acta B* 99 (2014) 82–86, <https://doi.org/10.1016/j.sab.2014.06.017>.
- [100] T. Yuan, Z. Wang, L. Li, Z. Hou, Z. Li, W. Ni, Quantitative carbon measurement in anthracite using laser-induced breakdown spectroscopy with binder, *Appl. Opt.* 51 (2012) B22–B29, <https://doi.org/10.1364/AO.51.000B22>.
- [101] M. Gaf, L. Nagli, I. Fasaki, M. Kompitsas, G. Wilsch, Laser-induced breakdown spectroscopy for on-line sulfur analyses of minerals in ambient conditions, *Spectrochim. Acta B* 64 (2009) 1098–1104, <https://doi.org/10.1016/j.sab.2009.07.010>.
- [102] V.S. Burakov, N.V. Tarasenko, M.I. Nedelko, V.A. Kononov, N.N. Vasilev, S. N. Isakov, Analysis of lead and sulfur in environmental samples by double pulse laser induced breakdown spectroscopy, *Spectrochim. Acta B* 64 (2009) 141–146, <https://doi.org/10.1016/j.sab.2008.11.005>.
- [103] J. Petrovic, J. Savovic, D. Rankovic, M. Kuzmanovic, Quantitative analysis of coal by laser induced breakdown spectroscopy using TEA CO<sub>2</sub> laser as the excitation source, *Plasma Chem. Plasma P.* 42 (2022) 519–533, <https://doi.org/10.1007/s11090-022-10234-6>.
- [104] W. Yin, L. Zhang, L. Dong, W. Ma, S. Jia, Design of a laser-induced breakdown spectroscopy system for on-line quality analysis of pulverized coal in power plants, *Appl. Spectrosc.* 63 (2009) 865–872, <https://doi.org/10.1366/000370209788964458>.
- [105] D. Body, B.L. Chadwick, Optimization of the spectral data processing in a LIBS simultaneous elemental analysis system, *Spectrochim. Acta B* 56 (2001) 725–736, [https://doi.org/10.1016/S0584-8547\(01\)00186-0](https://doi.org/10.1016/S0584-8547(01)00186-0).
- [106] F.J. Wallis, B.L. Chadwick, R.J.S. Morrison, Analysis of lignite using laser-induced breakdown spectroscopy, *Appl. Spectrosc.* 54 (2000) 1231–1235, <https://doi.org/10.1366/00037020019550814>.
- [107] W. Zhang, Z. Zhuo, P. Lu, J. Lu, T. Sun, J. Tang, H. Tang, T. Zhou, L. Li, Laser-induced breakdown spectroscopy for quantitative and qualitative analysis of the ash fusion temperatures of coal in power plants, *J. Anal. Atom. Spectrom.* 36 (2021) 576–589, <https://doi.org/10.1039/D0JA00453G>.
- [108] C.E. Romero, R. De Saro, J. Craparo, A. Weisberg, R. Moreno, Z. Yao, Laser-induced breakdown spectroscopy for coal characterization and assessing slagging propensity, *Energy Fuel* 24 (2010) 510–517, <https://doi.org/10.1021/ef900873w>.
- [109] Y. Jiang, Z. Lu, X. Chen, Z. Yu, H. Qin, J. Chen, J. Lu, S. Yao, Optimizing the quantitative analysis of solid biomass fuel properties using laser induced breakdown spectroscopy (LIBS) coupled with a kernel partial least squares (KPLS) model, *Anal. Methods* 13 (2021) 5467–5477, <https://doi.org/10.1039/d1ay01639c>.
- [110] X. Liu, X. Feng, L. Huang, Y. He, Rapid determination of wood and rice husk pellets' proximate analysis and heating value, *Energies* 13 (2020) 3741, <https://doi.org/10.3390/en13143741>.
- [111] Z. Lu, X. Chen, Y. Jiang, Z.X. Li, J. Chen, Y. Li, W. Lu, J. Lu, S. Yao, Application of laser induced breakdown spectroscopy for direct and quick determination of fuel property of woody biomass pellets, *Renew. Energy* 164 (2021) 1204–1214, <https://doi.org/10.1016/j.renene.2020.10.112>.
- [112] K.J. Larsen, A.D. Burns, S.R. Gubba, D.B. Ingham, L. Ma, M. Pourkashanian, A. Williams, Pulverised coal and biomass co-combustion: particle flow modelling in a swirl burner, *J. Energy Inst.* 86 (2013) 220–226, <https://doi.org/10.1179/1743967113Z.00000000065>.
- [113] T. Loree, L. Radziemski, Laser-induced breakdown spectroscopy: time-integrated applications, *Plasma Chem. Plasma P.* 1 (1981) 271–279, <https://doi.org/10.1007/BF00568835>.
- [114] D.K. Ottesen, L. Baxter, L. Radziemski, J. Burrows, Laser spark emission spectroscopy for in-situ, real-time monitoring of pulverized coal particle composition, *Energy Fuel* 5 (1991) 304–312, <https://doi.org/10.1021/ef00026a014>.
- [115] H. Zhang, J.P. Singh, F.-Y. Yueh, R.L. Cook, Laser-induced breakdown spectra in a coal-fired MHD facility, *Appl. Spectrosc.* 49 (1995) 1617–1623, <https://doi.org/10.1366/0003702953965759>.
- [116] S. Yao, L. Zhang, K. Yin, K. Bai, J. Xu, Z. Lu, J. Lu, Identifying laser-induced plasma emission spectra of particles in a gas–solid flow based on the standard deviation of intensity across an emission line, *J. Anal. Atom. Spectrom.* 33 (2018) 1676–1682, <https://doi.org/10.1039/C8JA00194D>.
- [117] J. Zheng, J. Lu, B. Zhang, M. Dong, S. Yao, W. Lu, X. Dong, Experimental study of laser-induced breakdown spectroscopy (LIBS) for direct analysis of coal particle flow, *Appl. Spectrosc.* 68 (2014) 672–679, <https://doi.org/10.1366/13-07278>.
- [118] Y. Chen, M. Dong, J. Cai, H. Chen, Z. Shang, J. Lu, An image auxiliary method for laser-induced breakdown spectroscopy analysis of coal particle flow, *J. Anal. Atom. Spectrom.* 37 (2022) 1126–1133, <https://doi.org/10.1039/D2JA00023G>.
- [119] S. Yao, J. Xu, X. Dong, B. Zhang, J. Zheng, J. Lu, Optimization of laser-induced breakdown spectroscopy for coal powder analysis with different particle flow diameters, *Spectrochim. Acta B* 110 (2015) 146–150, <https://doi.org/10.1016/j.sab.2015.06.011>.
- [120] S. Yao, J. Mo, J. Zhao, Y. Li, X. Zhang, W. Lu, Z. Lu, Development of a rapid coal analyzer using laser-induced breakdown spectroscopy (LIBS), *Appl. Spectrosc.* 72 (2018) 1225–1233, <https://doi.org/10.1177/0003702818772856>.
- [121] Z. Yu, S. Yao, L. Zhang, Z. Lu, Z. Lie, J. Lu, Surface-enhanced laser-induced breakdown spectroscopy utilizing metallic target for direct analysis of particle flow, *J. Anal. Atom. Spectrom.* 34 (2019) 172–179, <https://doi.org/10.1039/C8JA00347E>.
- [122] S. Yao, Z. Yu, S. Xu, X. Yao, H. Qin, Z. Lu, J. Lu, Repeatability improvement in laser induced plasma emission of particle flow by aberration-diminished focusing, *Spectrochim. Acta B* 175 (2021), 106014, <https://doi.org/10.1016/j.sab.2020.106014>.
- [123] N.V. Russell, L.B. Mendez, F. Wigley, J. Williamson, Ash deposition of a Spanish anthracite: effects of included and excluded mineral matter, *Fuel* 81 (2002) 657–663, [https://doi.org/10.1016/S0016-2361\(01\)00155-7](https://doi.org/10.1016/S0016-2361(01)00155-7).
- [124] Z. Wang, Y. Deguchi, M. Kuwahara, T. Taira, X. Zhang, J. Yan, J. Liu, H. Watanabe, R. Kurose, Quantitative elemental detection of size-segregated particles using laser-induced breakdown spectroscopy, *Spectrochim. Acta B* 87 (2013) 130–138, <https://doi.org/10.1016/j.sab.2013.05.034>.
- [125] Z. Yu, S. Yao, Y. Jiang, W. Chen, S. Xu, H. Qin, Z. Lu, J. Lu, Comparison of the matrix effect in laser induced breakdown spectroscopy analysis of coal particle flow and coal pellets, *J. Anal. Atom. Spectrom.* 36 (2021) 2473, <https://doi.org/10.1039/d1ja00223f>.
- [126] S.E. Hosseini, E. Owens, J. Krohn, J. Leyle, Experimental investigation into the effects of thermal recuperation on the combustion characteristics of a non-premixed meso-scale vortex combustor, *Energies* 11 (2018) 3390, <https://doi.org/10.3390/en11123390>.
- [127] H.I. Matheka, B.O. Oboirien, A. Engelbrecht, B.C. North, K. Premlal, Performance evaluation of south african coals under oxy-fuel combustion in a fluidized bed reactor, *Energy Fuel* 30 (2016) 6756–6763, <https://doi.org/10.1021/acs.energyfuels.6b00430>.
- [128] Z. Song, X. Zhang, X. Hou, M. Li, Effect of initial pressure, temperature and equivalence ratios on laminar combustion characteristics of hydrogen enriched natural gas, *J. Energy Inst.* 91 (2018) 887–893, <https://doi.org/10.1016/j.joei.2017.09.007>.
- [129] M. Carnogurska, M. Prihoda, M. Kosko, R. Pyszko, Verification of pollutant creation model at dendromass combustion, *J. Mech. Sci. Technol.* 26 (2012) 4161–4169, <https://doi.org/10.1007/s12206-012-0877-6>.
- [130] F. Ren, H. Chu, L. Xiang, W. Han, M. Gu, Effect of hydrogen addition on the laminar premixed combustion characteristics the main components of natural gas, *J. Energy Inst.* 92 (2019) 1178–1190, <https://doi.org/10.1016/j.joei.2018.05.011>.
- [131] A. Keromnes, W.K. Metcalfe, K.A. Heufer, N. Donohoe, A.K. Das, C. Sung, J. Herzler, C. Naumann, P. Griebel, O. Mathieu, An experimental and detailed chemical kinetic modeling study of hydrogen and syngas mixture oxidation at

- elevated pressures, *Combust. Flame*. 160 (2013) 995–1011, <https://doi.org/10.1016/j.combustflame.2013.01.001>.
- [132] A.G. Tereshchenko, D.A. Knyaz'kov, P.A. Skovorodko, A.A. Paletsky, O. P. Korobeinichev, Perturbations of the flame structure due to a thermocouple, *Combust. Explo. Shock*. 47 (2011) 403–413, <https://doi.org/10.1134/S0010508211040034>.
- [133] S. Krishnan, B.M. Kumfer, W. Wu, J. Li, A. Nehorai, R.L. Axelbaum, An approach to thermocouple measurements that reduces uncertainties in high-temperature environments, *Energy Fuel* 29 (2015) 3446–3455, <https://doi.org/10.1021/acs.energyfuels.5b00071>.
- [134] M.F. Modest, *Radiative heat transfer*, 2nd ed., Academic Press, Burlington, 2003.
- [135] H. Zhou, X. Lou, J. Xiao, H. Yin, G. Sun, Experimental study on image processing of flame temperature distribution in a pilot-scale furnace, *Proceed. CSEE* 15 (5) (1995) 295–300.
- [136] D.P. DeWitt, G.D. Nutter, *Theory and practice of radiation thermometry*, John Wiley & Sons, New Jersey, 1991.
- [137] Y. Sun, C. Lou, H. Zhou, A simple judgment method of gray property of flames based on spectral analysis and the two-color method for measurements of temperatures and emissivity, *P Combust. Inst.* (2011) 33735–33741, <https://doi.org/10.1016/j.proci.2010.07.042>.
- [138] B. Goktepe, K. Umeki, R. Gebart, Does distance among biomass particles affect soot formation in an entrained flow gasification process? *Fuel Process. Technol.* 141 (2016) 99–105, <https://doi.org/10.1016/j.fuproc.2015.06.038>.
- [139] W. Jing, Z. Wu, W. Zhang, T. Fang, Measurements of soot temperature and KL factor for spray combustion of biomass derived renewable fuels, *Energy*. 91 (2015) 758–771, <https://doi.org/10.1016/j.energy.2015.08.069>.
- [140] H. Liu, S. Zheng, H. Zhou, C. Qi, Measurement of distributions of temperature and wavelength-dependent emissivity of a laminar diffusion flame using hyperspectral imaging technique, *Meas. Sci. Technol.* 27 (2016), 025201, <https://doi.org/10.1088/0957-0233/27/2/025201>.
- [141] H. Liu, S. Zheng, H. Zhou, Measurement of soot temperature and volume fraction of axisymmetric ethylene laminar flames using hyperspectral tomography, *Ieee T Instrum. Meas.* 66 (2017) 315–324, <https://doi.org/10.1109/TIM.2016.2631798>.
- [142] W. Yan, S. Zheng, H. Zhou, Experiments investigation on 2D distribution of soot temperature and volume fraction by image processing of visible radiation, *Appl. Therm. Eng.* 124 (2017) 1014–1022, <https://doi.org/10.1016/j.applthermaleng.2017.06.087>.
- [143] H. Liu, H. Zhou, C. Xu, A decomposition method for the simultaneous reconstruction of temperature and soot volume fraction distributions in axisymmetric flames, *Meas. Sci. Technol.* 31 (2020), 115202, <https://doi.org/10.1088/1361-6501/ab9dbf>.
- [144] H. Zhou, C. Lou, C. Qiang, Z. Jiang, H. Jin, B. Huang, Z. Pei, C. Lu, Experimental investigations on visualization of three-dimensional temperature distributions in a large-scale pulverized-coal-fired boiler furnace, *P Combust. Inst.* 30 (2005) 1699–1706, <https://doi.org/10.1016/j.proci.2004.08.090>.
- [145] Q. Cheng, X. Zhang, Z. Wang, H. Zhou, S. Shao, Simultaneous measurement of three-dimensional temperature distributions and radiative properties based on radiation image processing technology in a gas-fired pilot tubular furnace, *Heat Transfer. Eng.* 35 (2014) 770–779, <https://doi.org/10.1080/08832323.2013.838096>.
- [146] X. Zhang, S. Zheng, H. Zhou, B. Zhang, H. Wang, H. Xu, Simultaneously reconstruction of inhomogeneous temperature and radiative properties by radiation image processing, *Int. J. Therm. Sci.* 107 (2016) 121–130, <https://doi.org/10.1016/j.ijthermalsci.2016.04.003>.
- [147] C. Hu, Y. Gong, Q. Guo, Y. Wang, G. Yu, Experimental study on the spectroscopy of opposed impinging diesel flames based on a bench-scale gasifier, *Energy Fuel* 31 (2017) 4469–4478, <https://doi.org/10.1021/acs.energyfuels.6b03239>.
- [148] C. Hu, Y. Gong, Q. Guo, X. Song, G. Yu, An experimental study on the spectroscopic characteristics in coal-water slurry diffusion flames based on hot-oxygen burner technology, *Fuel Process. Technol.* 154 (2016) 168–177, <https://doi.org/10.1016/j.fuproc.2016.08.029>.
- [149] N. Desmira, T. Nagasaka, K. Narukawa, Spectroscopic observation of chemical species from high-temperature air pulverized coal combustion, *J. Energ. Resour.-Asme*. 135 (2013), 034503, <https://doi.org/10.1115/1.4024120>.
- [150] G. Hidegh, V. Jozsa, Correlation analysis of chemiluminescent and pollutant emissions of a liquid-fueled turbulent swirl burner, *J. Energy Inst.* 94 (2020) 1390–1398, <https://doi.org/10.1016/j.joei.2020.01.001>.
- [151] W. Bakker, G. Stanko, J. Blough, W. Seitz, S. Niksa, Waterwall corrosion in pulverized coal burning boilers: root causes and wastage predictions, *Mater. High Temp.* 24 (2007) 275–284, <https://doi.org/10.3184/096034007X278356>.
- [152] T. Zhang, Q. Guo, Q. Liang, Z. Dai, G. Yu, Distribution characteristics of OH\*, CH\*, and C<sub>2</sub>\* luminescence in CH<sub>4</sub>/O<sub>2</sub> co-flow diffusion flames, *Energy Fuel* 26 (2012) 5503–5508, <https://doi.org/10.1021/ef300970a>.
- [153] J. Krabicka, G. Lu, Y. Yan, Profiling and characterization of flame radicals by combining spectroscopic imaging and neural network techniques, *Ieee T Instrum. Meas.* 60 (2011) 1854–1860, <https://doi.org/10.1109/TIM.2010.2102411>.
- [154] S.S. Merola, C. Tornatore, S.E. Iannuzzi, L. Marchitto, G. Valentino, Combustion process investigation in a high speed diesel engine fuelled with n-butanol diesel blend by conventional methods and optical diagnostics, *Renew. Energy* 64 (2014) 225–237, <https://doi.org/10.1016/j.renene.2013.11.017>.
- [155] N. Desmira, K. Kuniyuki, S. Morita, A.K. Gupta, In-situ spectroscopic monitoring of Jatropha oil combustion properties, *Renew. Energy* 63 (2014) 775–778, <https://doi.org/10.1016/j.renene.2013.10.020>.
- [156] A.I. Barros, A.P. de Oliveira, M.R.L. de Magalhaes, R.D. Villa, Determination of sodium and potassium in biodiesel by flame atomic emission spectrometry, with dissolution in ethanol as a single sample preparation step, *Fuel*. 93 (2012) 381–384, <https://doi.org/10.1016/j.fuel.2011.08.060>.
- [157] C. Hu, Q. Guo, Y. Gong, L. He, G. Yu, Alkalis atomic emission spectroscopy and flame temperature measurement of diesel impinging flames in an opposed multi-burner gasifier, *Exp. Thermal Fluid Sci.* 98 (2018) 445–453, <https://doi.org/10.1016/j.exptthermfluidsci.2018.06.028>.
- [158] P.E. Mason, L.L. Darvell, J.M. Jones, A. Williams, Observations on the release of gas-phase potassium during the combustion of single particles of biomass, *Fuel*. 182 (2016) 110–117, <https://doi.org/10.1016/j.fuel.2016.05.077>.
- [159] P.E. Mason, J.M. Jones, L.L. Darvell, A. Williams, Gas phase potassium release from a single particle of biomass during high temperature combustion, *P Combust. Inst.* 36 (2017) 2207–2215, <https://doi.org/10.1016/j.proci.2016.06.020>.
- [160] M. Lim, L. Matsuoka, In-situ quantification of alkali metals from biomass combustion by optical emission spectroscopy, *Iop Conf. Ser.: Mater. Sci. Eng.* 736 (2020), 022043, <https://doi.org/10.1088/1757-899X/736/2/022043>.
- [161] W. Weng, M. Costa, Z. Li, M. Alden, Temporally and spectrally resolved images of single burning pulverized wheat straw particles, *Fuel*. 224 (2018) 434–441, <https://doi.org/10.1016/j.fuel.2018.03.101>.
- [162] W. Weng, M. Costa, M. Alden, Z. Li, Single particle ignition and combustion of pulverized pine wood, wheat straw, rice husk and grape pomace, *P Combust. Inst.* 37 (2019) 2663–2671, <https://doi.org/10.1016/j.proci.2018.05.095>.
- [163] S. Li, M. Dong, J. Lu, Z. Tian, Z. Hou, W. Lin, B. Yu, Q. Lai, S. Chen, J. Qiu, Study on the alkali release from the combustion products of a single coal particle by laser ignition, *Energy Fuel* 31 (2017) 4452–4460, <https://doi.org/10.1021/acs.energyfuels.6b03174>.
- [164] M. Dong, F. Luo, M. Huang, S. Li, W. Zhao, J. Lu, Study on the ignition characteristics and alkali release of single coal particles with additional different forms of potassium, *Fuel Process. Technol.* 203 (2020), 106385, <https://doi.org/10.1016/j.fuproc.2020.106385>.
- [165] M.M. Sentko, S. Schulz, B. Stelzner, C. Anderlohr, M. Vicari, D. Trimis, Determination of temperature and water-concentration in fuel-rich oxy-fuel methane flames applying TDLAS, *Combust. Flame*. 214 (2020) 336–345, <https://doi.org/10.1016/j.combustflame.2020.01.003>.
- [166] Y. Zhang, B. Xiao, Y. Li, P. Liu, R. Zhan, Z. Huang, H. Lin, LIF diagnostics for selective and quantitative measurement of PAHs in laminar premixed flames, *Combust. Flame*. 222 (2020) 5–17, <https://doi.org/10.1016/j.combustflame.2020.08.018>.
- [167] F. Vestin, M. Afzelius, P.-E. Bengtsson, Development of rotational CARS for combustion diagnostics using a polarization approach, *P Combust. Inst.* 31 (2007) 833–840, <https://doi.org/10.1016/j.proci.2006.07.066>.
- [168] F. Ferioli, S. Buckley, Measurements of hydrocarbons using laser-induced breakdown spectroscopy, *Combust. Flame*. 144 (2006) 435–447, <https://doi.org/10.1016/j.combustflame.2005.08.005>.
- [169] P. Stavropoulos, G. Skevis, S. Couris, Global and local equivalence ratio measurements in laminar premixed hydrocarbon-air flames using laser induced breakdown spectroscopy (LIBS), *Proceedings of the European Combustion Meeting, Belgium (2005)* 3–6.
- [170] M. Mansour, H. Imam, K.A. Elsayed, A.M. Elbaz, W. Abbass, Quantitative mixture fraction measurements in combustion system via laser induced breakdown spectroscopy, *Opt. Laser Technol.* 65 (2015) 43–49, <https://doi.org/10.1016/j.optlastec.2014.07.005>.
- [171] M.S. Mansour, H. Imam, K.A. Elsayed, W. Abbass, Local equivalence ratio measurements in turbulent partially premixed flames using laser-induced breakdown spectroscopy, *Spectrochim. Acta B* 64 (2009) 1079–1084, <https://doi.org/10.1016/j.sab.2009.07.022>.
- [172] L. Zimmer, S. Tachibana, Laser induced plasma spectroscopy for local equivalence ratio measurements in an oscillating combustion environment, *P Combust. Inst.* 31 (2007) 737–745, <https://doi.org/10.1016/j.proci.2006.07.035>.
- [173] J. Kiefer, C. Vanselow, A. Fischer, Combining laser-induced breakdown spectroscopy (LIBS) and particle imaging velocimetry (PIV) for flame diagnostics, *Laser Applic. Chem. Secur. Environ. Anal.* (2020), <https://doi.org/10.1364/LACSEA-2020-LW4E.3.LW4E.3>.
- [174] S.H. Lee, H.T. Hahn, J.J. Yoh, Towards a two-dimensional laser induced breakdown spectroscopy mapping of liquefied petroleum gas and electrolytic oxy-hydrogen flames, *Spectrochim. Acta B* 88 (2013) 63–68, <https://doi.org/10.1016/j.sab.2013.08.005>.
- [175] Y. Wu, M. Gragston, Z. Zhang, P.S. Hsu, N. Jiang, A.K. Patnaik, S. Roy, J.R. Gord, High-pressure 1D fuel/air-ratio measurements with LIBS, *Combust. Flame*. 198 (2018) 120–129, <https://doi.org/10.1016/j.combustflame.2018.09.009>.
- [176] T.-W. Lee, N. Hegde, Laser-induced breakdown spectroscopy for in situ diagnostics of combustion parameters including temperature, *Combust. Flame*. 142 (2005) 314–316, <https://doi.org/10.1016/j.combustflame.2005.05.003>.
- [177] J. Kiefer, J.W. Tröger, Z. Li, T. Seeger, M. Alden, A. Leipertz, Laser-induced breakdown flame thermometry, *Combust. Flame*. 159 (2012) 3576–3582, <https://doi.org/10.1016/j.combustflame.2012.08.005>.
- [178] A.P. Williamson, U. Thiele, J. Kiefer, Comparison of existing laser-induced breakdown thermometry techniques along with a time-resolved breakdown approach, *Appl. Opt.* 58 (2019) 3950–3956, <https://doi.org/10.1364/AO.58.003950>.
- [179] W. Wu, A. Adeosun, R.L. Axelbaum, A new method of flame temperature measurement utilizing the acoustic emissions from laser-induced plasmas, *P Combust. Inst.* 37 (2019) 1409–1415, <https://doi.org/10.1016/j.proci.2018.07.096>.

- [180] Z. Tian, M. Dong, S. Li, J. Lu, Spatially resolved laser-induced breakdown spectroscopy in laminar premixed methane-air flames, *Spectrochim. Acta B* 136 (2017) 8–15, <https://doi.org/10.1016/j.sab.2017.08.001>.
- [181] J.H. Kim, S.H. Lee, H. Do, J.J. Yoh, Instantaneous monitoring of local fuel concentration in a liquid hydrocarbon-fueled flame using a LIBS plug, *Energy* 140 (2017) 18–26, <https://doi.org/10.1016/j.energy.2017.08.081>.
- [182] B. Li, D. Zhang, J. Liu, Y. Tian, Q. Gao, Z. Li, A review of femtosecond laser-induced emission techniques for combustion and flow field diagnostics, *Appl. Sci.* 9 (9) (2019), <https://doi.org/10.3390/app9091906>.
- [183] M. Kotzagianni, S. Couris, Femtosecond laser induced breakdown for combustion diagnostics, *Appl. Phys. A-Mater Lett.* 100 (2012), 264104, <https://doi.org/10.1063/1.4731781>.
- [184] S. Couris, M. Kotzagianni, A. Baskevicius, T. Bartulevicius, V. Sirutkaitis, Combustion diagnostics with femtosecond laser radiation, *J. Phys. Conf. Ser.* 548 (2014), 012056, <https://doi.org/10.1088/1742-6596/548/1/012056>.
- [185] H. Zang, D. Yao, S. Wang, Y. Fu, W. Zhang, S. Chen, H. Li, H. Xu, In situ determination of the equivalence ratio in a methane/air flow field by femtosecond filament excitation, *Laser Phys.* 30 (2020), 035402, <https://doi.org/10.1088/1555-6611/ab6aa6>.
- [186] B. Li, D. Zhang, Q. Gao, Z. Li, One-dimensional full-range mixture fraction measurements with femtosecond laser-induced plasma spectroscopy, *Exp. Fluids* 61 (2020) 1–9, <https://doi.org/10.1007/s00348-020-2877-0>.
- [187] D. Zhang, Q. Gao, B. Li, Z. Zhu, Z. Li, Instantaneous one-dimensional equivalence ratio measurements in methane/air mixtures using femtosecond laser-induced plasma spectroscopy, *Opt. Express* 27 (2019) 2159–2169, <https://doi.org/10.1364/OE.27.0202159>.
- [188] H. Li, X. Wei, H. Xu, S. Chin, K. Yamanouchi, H. Sun, Femtosecond laser filamentation for sensing combustion intermediates: a comparative study, *Sensor Actua B-Chem.* 203 (2014) 887–890, <https://doi.org/10.1016/j.snb.2014.06.086>.
- [189] L.J. Hsu, Z.T. Alwahabi, G.J. Nathan, P.J. Ashman, G.J. Nathan, Y. Li, Z. Li, M. Aldén, Study of the quantitative release of sodium and potassium from brown coal and pine wood in a laminar pre-mixed methane flame using LIBS, in: *Proceedings of 2009 Annual Bulletin of the Australian Institute of High Energetic Materials*, 2010, pp. 17–22.
- [190] L.J. Hsu, Z.T. Alwahabi, G.J. Nathan, Y. Li, Z. Li, M. Aldén, Sodium and potassium released from burning particles of brown coal and pine wood in a laminar premixed methane flame using quantitative laser-induced breakdown spectroscopy, *Appl. Spectrosc.* 65 (2011) 684–691, <https://doi.org/10.1366/10-06108>.
- [191] Y. Li, H. Zhang, Z. Li, H. Li, C. Zhang, C. Hu, In situ analysis of Na and K in a laminar premixed flame by laser-induced breakdown spectroscopy, *Chem. Res. Chin. U.* 29 (2013) 1149–1152, <https://doi.org/10.1007/s40242-013-3268-3>.
- [192] Y. He, J. Zhu, B. Li, Z. Wang, Z. Li, M. Aldén, K. Cen, In-situ measurement of sodium and potassium release during oxy-fuel combustion of lignite using laser-induced breakdown spectroscopy: effects of O<sub>2</sub> and CO<sub>2</sub> concentration, *Energy Fuel* 27 (2013) 1123–1130, <https://doi.org/10.1021/ef301750h>.
- [193] Y. He, K. Qiu, R. Whiddon, Z. Wang, Y. Zhu, Y. Liu, Z. Li, K. Cen, Release characteristic of different classes of sodium during combustion of Zhun-Dong coal investigated by laser-induced breakdown spectroscopy, *Sci. Bull.* 60 (2015) 1927–1934, <https://doi.org/10.1007/s11434-015-0922-9>.
- [194] Y. He, R. Whiddon, Z. Wang, Y. Liu, Y. Zhu, J. Liu, K. Cen, Inhibition of sodium release from zhundong coal via the addition of mineral additives: online combustion measurement with laser-induced breakdown spectroscopy (LIBS), *Energy Fuel* 31 (2017) 1082–1090, <https://doi.org/10.1021/acs.energyfuels.6b01673>.
- [195] Z. Wang, Y. Liu, Y. He, R. Whiddon, K. Wan, J. Xia, J. Liu, Effects of microwave irradiation on combustion and sodium release characteristics of zhundong lignite, *Energy Fuel* 30 (2016) 8977–8984, <https://doi.org/10.1021/acs.energyfuels.6b01494>.
- [196] Y. Liu, Y. He, Z. Wang, J. Xia, K. Wan, R. Whiddon, K. Cen, Characteristics of alkali species release from a burning coal/biomass blend, *Appl. Energy* 215 (2018) 523–531, <https://doi.org/10.1016/j.apenergy.2018.02.015>.
- [197] Z. Zhang, Q. Song, Z.T. Alwahabi, Q. Yao, G.J. Nathan, Temporal release of potassium from pinewood particles during combustion, *Combust. Flame* 162 (2015) 496–505, <https://doi.org/10.1016/j.combustflame.2014.07.030>.
- [198] H. Fatehi, Y. He, Z. Wang, Z.S. Li, X.S. Bai, M. Aldén, K.F. Cen, LIBS measurements and numerical studies of potassium release during biomass gasification, *P Combust. Inst.* 35 (2015) 2389–2396, <https://doi.org/10.1016/j.proci.2014.06.115>.
- [199] O. Chansa, Z. Luo, E.G. Eddings, C. Yu, Determination of alkali release during oxyfuel co-combustion of biomass and coal using laser-induced breakdown spectroscopy, *Fuel* 289 (2021), 119658, <https://doi.org/10.1016/j.fuel.2020.119658>.
- [200] P.J. Van Eyk, P.J. Ashman, G.J. Nathan, Mechanism and kinetics of sodium release from brown coal char particles during combustion, *Combust. Flame* 158 (2011) 2512–2523, <https://doi.org/10.1016/j.combustflame.2011.05.005>.
- [201] Y. Liu, Z. Wang, Y. Lv, K. Wan, Y. He, J. Xia, K. Cen, Inhibition of sodium release from Zhundong coal via the addition of mineral additives: a combination of online multi-point LIBS and offline experimental measurements, *Fuel* 212 (2018) 498–505, <https://doi.org/10.1016/j.fuel.2017.10.081>.
- [202] Y. Liu, Z. Wang, K. Wan, Y. Lv, J. Xia, Y. He, K. Cen, In situ measurements of the release characteristics and catalytic effects of different chemical forms of sodium during combustion of Zhundong coal, *Energy Fuel* 32 (2018) 6595–6602, <https://doi.org/10.1021/acs.energyfuels.8b00773>.
- [203] Y. Liu, Y. He, Z. Wang, K. Wan, J. Xia, J. Liu, K. Cen, Multi-point LIBS measurement and kinetics modeling of sodium release from a burning Zhundong coal particle, *Combust. Flame* 189 (2018) 77–86, <https://doi.org/10.1016/j.combustflame.2017.10.026>.
- [204] Y. Liu, Z. Wang, J. Xia, L. Vervisch, K. Wan, Y. He, R. Whiddon, H. Bahai, K. Cen, Measurement and kinetics of elemental and atomic potassium release from a burning biomass pellet, *P Combust. Inst.* 37 (2019) 2681–2688, <https://doi.org/10.1016/j.proci.2018.06.042>.
- [205] S. Li, M. Dong, F. Luo, W. Li, L. Wei, J. Lu, Experimental investigation of combustion characteristics and NOx formation of coal particles using laser induced breakdown spectroscopy, *J. Energy Inst.* 93 (2020) 52–61, <https://doi.org/10.1016/j.joei.2019.04.009>.
- [206] Y. Yuan, S. Li, Q. Yao, Dynamic behavior of sodium release from pulverized coal combustion by phase-selective laser-induced breakdown spectroscopy, *P Combust. Inst.* 35 (2015) 2339–2346, <https://doi.org/10.1016/j.proci.2014.07.016>.
- [207] Q. Gao, S. Li, Y. Yuan, Y. Zhang, Q. Yao, Ultrafine particulate matter formation in the early stage of pulverized coal combustion of high-sodium lignite, *Fuel* 158 (2015) 224–231, <https://doi.org/10.1016/j.fuel.2015.05.028>.
- [208] Y. Zhang, S. Li, Y. Ren, Q. Yao, C.K. Law, Two-dimensional imaging of gas-to-particle transition in flames by laser-induced nanoplasmas, *Appl. Phys. A-Mater. Lett.* 104 (2014), 023115, <https://doi.org/10.1063/1.4861904>.
- [209] Y. Zhang, G. Xiong, S. Li, Z. Dong, S.G. Buckley, S.D. Tse, Novel low-intensity phase-selective laser-induced breakdown spectroscopy of TiO<sub>2</sub> nanoparticle aerosols during flame synthesis, *Combust. Flame* 160 (2013) 725–733, <https://doi.org/10.1016/j.combustflame.2012.11.007>.
- [210] Y. Zhang, S. Li, Y. Ren, Q. Yao, S.D. Tse, A new diagnostic for volume fraction measurement of metal-oxide nanoparticles in flames using phase-selective laser-induced breakdown spectroscopy, *P Combust. Inst.* 35 (2015) 3681–3688, <https://doi.org/10.1016/j.proci.2014.06.018>.
- [211] J.C. Hower, J.G. Groppo, U.M. Graham, C.R. Ward, I.J. Kostova, M.M. Maroto-Valer, S. Dai, Coal-derived unburned carbons in fly ash: a review, *Int. J. Coal Geol.* 179 (2017) 11–27, <https://doi.org/10.1016/j.coal.2017.05.007>.
- [212] F. Cangialosi, M. Notarnicola, L. Liberti, J.M. Stencel, The effects of particle concentration and charge exchange on fly ash beneficiation with pneumatic triboelectrostatic separation, *Sep. Purif. Technol.* 62 (2008) 240–248, <https://doi.org/10.1016/j.seppur.2008.01.031>.
- [213] K. Pedersen, A. Jensen, M. Skjothrasmussen, K. Damjohansen, A review of the interference of carbon containing fly ash with air entrainment in concrete, *Prog. Energy. Combust.* 34 (2008) 135–154, <https://doi.org/10.1016/j.pecs.2007.03.002>.
- [214] P. Chindaprasit, U. Rattanasak, S. Taebuanhuad, Role of microwave radiation in curing the fly ash geopolymer, *Adv. Powder Technol.* 24 (2013) 703–707, <https://doi.org/10.1016/j.apt.2012.12.005>.
- [215] T. Ctvrtnickova, M.-P. Mateo, A. Yañez, G. Nicolas, Characterization of coal fly ash components by laser-induced breakdown spectroscopy, *Spectrochim. Acta B* 64 (2009) 1093–1097, <https://doi.org/10.1016/j.sab.2009.07.032>.
- [216] A. Stankova, N. Gilon, L. Dutruch, V. Kanicky, A simple LIBS method for fast quantitative analysis of fly ashes, *Fuel* 89 (2010) 3468–3474, <https://doi.org/10.1016/j.fuel.2010.06.018>.
- [217] S. Yao, J. Lu, J. Zheng, M. Dong, Analyzing unburned carbon in fly ash using laser-induced breakdown spectroscopy with multivariate calibration method, *J. Anal. Atom. Spectrom.* 27 (2012) 473–478, <https://doi.org/10.1039/C2JA10229C>.
- [218] S. Yao, X. Yao, L. Zhang, H. Qin, Z. Yu, X. Chen, Z. Lu, J. Lu, Improving the LIBSs quantitative analysis of unburned carbon in fly ash based on the optimization of reference value, *Energy Fuel* 34 (2020) 6483–6489, <https://doi.org/10.1021/acs.energyfuels.0c00298>.
- [219] K. Bai, S. Yao, J. Lu, J. Zhao, J. Xu, Z. Lu, Correction of C-Fe line interference for the measurement of unburned carbon in fly ash by LIBS, *J. Anal. Atom. Spectrom.* 31 (2016) 2418–2426, <https://doi.org/10.1039/C6JA00307A>.
- [220] S. Yao, Y. Shen, K. Yin, G. Pan, J. Lu, Rapidly measuring unburned carbon in fly ash using molecular CN by laser-induced breakdown spectroscopy, *Energy Fuel* 29 (2015) 1257–1263, <https://doi.org/10.1021/ef502174q>.
- [221] M. Noda, Y. Deguchi, S. Iwasaki, N. Yoshikawa, Detection of carbon content in a high-temperature and high-pressure environment using laser-induced breakdown spectroscopy, *Spectrochim. Acta B* 57 (2002) 701–709, [https://doi.org/10.1016/S0584-8547\(01\)00403-7](https://doi.org/10.1016/S0584-8547(01)00403-7).
- [222] M. Kurihara, K. Ikeda, Y. Izawa, Y. Deguchi, H. Tarui, Optimal boiler control through real-time monitoring of unburned carbon in fly ash by laser-induced breakdown spectroscopy, *Appl. Opt.* 42 (2003) 6159–6165, <https://doi.org/10.1364/AO.42.006159>.
- [223] L. Zhang, W. Ma, L. Dong, X. Yan, Z. Hu, Z. Li, Y. Zhang, L. Wang, W. Yin, S. Jia, Development of an apparatus for on-line analysis of unburned carbon in fly ash using laser-induced breakdown spectroscopy (LIBS), *Appl. Spectrosc.* 65 (2011) 790–796, <https://doi.org/10.1366/10-06213>.
- [224] Z. Wang, Y. Deguchi, H. Watanabe, R. Kurose, J. Yan, J. Liu, Improvement on quantitative measurement of fly ash contents using laser-induced breakdown spectroscopy, *J. Flow Contr. Measure. Visual.* 03 (2015) 10–21, <https://doi.org/10.4236/jfcmv.2015.31002>.
- [225] Z. Wang, R. Liu, Y. Deguchi, S. Tanaka, K. Tainaka, K. Tanno, J. Yan, J. Liu, H. Watanabe, Detection improvement of unburned carbon content in fly ash flow using LIBS with a two-stage cyclone measurement system, *Energy Fuel* 33 (2019) 7805–7812, <https://doi.org/10.1021/acs.energyfuels.9b01161>.